Dark Matter Search in a Beam-Dump Experiment Utilizing a Low-Threshold, Directional Dark Matter Detector (BDX-DRIFT) at Jefferson Lab

D. Snowden-Ifft[1,2], J.-L. Gauvreau, G. Gregory, N. Ma
Occidental College, Los Angeles, California 90041, USA

J. Harton[2], F. Schuckman, D. Warner
Department of Physics, Colorado State University, Fort Collins, Colorado 80523, USA

I. Jaeglé
University of Florida, Gainesville Florida 32611, USA

M. Battaglieri[2], A. Bersani, B. Cai, A. Celentano, R. De Vita, E. Fanchini, L. Marsicano, P. Musico, M. Osipenko, F. Panza, M. Ripani, E. Santopinto, M. Taiuti
Istituto Nazionale di Fisica Nucleare, Sezione di Genova
e Dipartimento di Fisica dell'Universitá, 16146 Genova, Italy

V. Bellini, M. Bondí, M. De Napoli, F. Mammoliti, E. Leonora, N. Randazzo, G. Russo, M. Sperduto, C. Sutera, F. Tortorici
Istituto Nazionale di Fisica Nucleare, Sezione di Catania, Catania, Italy

N.Baltzell, M. Dalton, A. Freyberger, F.-X. Girod, V. Kubarovsky, E. Pasyuk, E. Smith[2], S. Stepanyan, M. Ungaro, T. Whitlatch
Jefferson Lab, Newport News, VA 23606, USA

G. Krnjaic
Center for Particle Astrophysics, Fermi National Accelerator Laboratory, Batavia, IL 60510

D. Loomba
University of New Mexico, Albuquerque, New Mexico, NM

M. Carpinelli, V. Sipala
Universit`a di Sassari e Istituto Nazionale di Fisica Nucleare, 07100 Sassari, Italy

[1] Contact Person, email: ifft@oxy.edu
[2] Spokesperson

P. Schuster, N. Toro
Stanford Linear Accelerator Center (SLAC), Menlo Park, CA 94025, US

R. Essig
C.N. Yang Inst. for Theoretical Physics, Stony Brook University, NY

M. Wood
Canisius College, Buffalo NY 14208, USA

M.Holtrop, R. Paremuzyan
University of New Hampshire, Durham NH 03824, USA

G. De Cataldo, R. De Leo, D. Di Bari, L. Lagamba, E. Nappi, R. Perrino
Istituto Nazionale di Fisica Nucleare, Sezione di Bari e Dipartimento di Fisica dell'Universitá, Bari, Italy

I. Balossino, L. Barion, G. Ciullo, M. Contalbrigo, P. Lenisa, A. Movsisyan, F. Spizzo, M. Turisini
Istituto Nazionale di Fisica Nucleare, Sezione di Ferrara e Dipartimento di Fisica ell'Universitá, Ferrara, Italy

F. De Persio, E. Cisbani, F. Garibaldi, F. Meddi, G. M. Urciuoli
Istituto Nazionale di Fisica Nucleare, Sezione di Roma e Gruppo Collegato Sanitá, e Universitá La Sapienza, Italy

D. Hasch, V. Lucherini, M. Mirazita, S. Pisano
Istituto Nazionale di Fisica Nucleare, Laboratori Nazionali di Frascati, P.O. 13, 00044 Frascati, Italy

G. Simi
Istituto Nazionale di Fisica Nucleare, Sezione di Padova, Padova, Italy

A. D'Angelo, L. Lanza, A. Rizzo, C. Schaerf, I. Zonta
Istituto Nazionale di Fisica Nucleare, Sezione di Roma-TorVergata e Dipartimento di Fisica dell'Universitá, Roma, Italy

A. Filippi
Istituto Nazionale di Fisica Nucleare, Sezione di Torino, Torino, Italy

S. Fegan
Institut fur Kernphysik, Johannes Gutenberg-Universität Mainz, 55128 Mainz, Germany

M. Kunkel

Nuclear Physics Institute and Juelich Center for Hadron Physics, Forschungszentrum Juelich, Germany

M. Bashkanov, P. Beltrame, A. Murphy, G. Smith, D. Watts, N. Zachariou, L. Zana
Edinburgh University, Edinburgh EH9 3JZ, United Kingdom

D. Glazier, D. Ireland, B. McKinnon, D. Sokhan
University of Glasgow, Glasgow G12 8QQ, United Kingdom

L. Colaneri
Institut de Physique Nucléaire d'Orsay, IN2P3, BP 1, 91406 Orsay, France

S. Anefalos Pereira
Instituto de Fisica, Universidade de São Paulo, Brasil

A. Afanasev, B. Briscoe, I. Strakovsky
The George Washington University, Washington, D.C., 20052

N. Kalantarians
Department of Physics, Hampton University, Hampton VA 23668, USA

L. Weinstein
Old Dominion University, Department of Physics, Norfolk VA 23529, USA

K. P. Adhikari, J. A. Dunne, D. Dutta, L. El Fassi, L. Ye
Mississippi State University, Mississippi State, MS 39762, USA

K. Hicks
Ohio University, Department of Physics, Athens, OH 45701, USA

P. Cole
Dept. of Physics, Idaho State University, Pocatello, ID 83201 USA

S. Dobbs
Northwestern University, Evanston, IL 60208, USA

C. Fanelli
Massachusetts Institute of Technology, Cambridge, MA 02139, USA

Abstract

Light dark matter (LDM) in the context of dark sector theories is an attractive candidate to make up the bulk of the mass of our Universe. This proposal presents the LDM discovery potential of a low-pressure, negative-ion, time-projection-chamber detector placed downstream of the Hall A beam-dump at Jefferson Lab receiving 10^{22} electrons on target (EOT) As with the approved Beam-Dump eXperiment (BDX) the Directional Recoil Identification From Tracks Beam-Dump eXperiment (DRIFT-BDX) would run parasitically and in parallel with BDX providing additional reach, confirmation potential and different backgrounds all providing a high degree of complementarity. DRIFT-BDX is sensitive to elastic nuclear recoil events with a threshold of ~1 keV/amu recoil energy. Multiple, powerful signatures of LDM interactions are possible with BDX-DRIFT detector. Detailed calculations are presented exploring cosmic ray and beam-related backgrounds. The proposed experiment will be sensitive to large regions of LDM parameter space, exceeding the discovery potential of existing and planned experiments in the MeV-GeV DM mass range.

Introduction

Despite decades of astounding experimental progress in direct searches for dark matter in the GeV-TeV mass-scale [1], there are no compelling detections to date. This absence of detections, together with the lack of any hint of supersymmetry at the LHC [2], places severe constraints on the minimal, most “natural”, dark matter models. That, in turn, has led both theorists and experimentalists to look beyond the classic, supersymmetry-motivated weakly interacting massive particle (WIMP) dark matter [3][4]. An interesting candidate scale is light dark matter (LDM) in the range MeV-GeV [5]. LDM finds a natural home in theories which postulate new MeV-GeV scale ‘dark’ force carriers [5] and are accessible at high intensity accelerators with specially designed detectors [4].

Dark Sectors and Light Dark Matter

Electron beam dump experiments have a history dating back to the 1980s [6]. Recently there has been renewed interest in them because they have been shown to have high sensitivity to LDM under the parameterization of dark sector theories [4][7][8][9][9]. A schematic, highlighting the major elements of a beam dump experiment, is shown in Figure 1. The 4 main elements of a beam dump experiment are 1) a multi-GeV electron beam, 2) an accelerator dump, 3) shielding to stop standard model particles produced in the dump and 4) a detector.

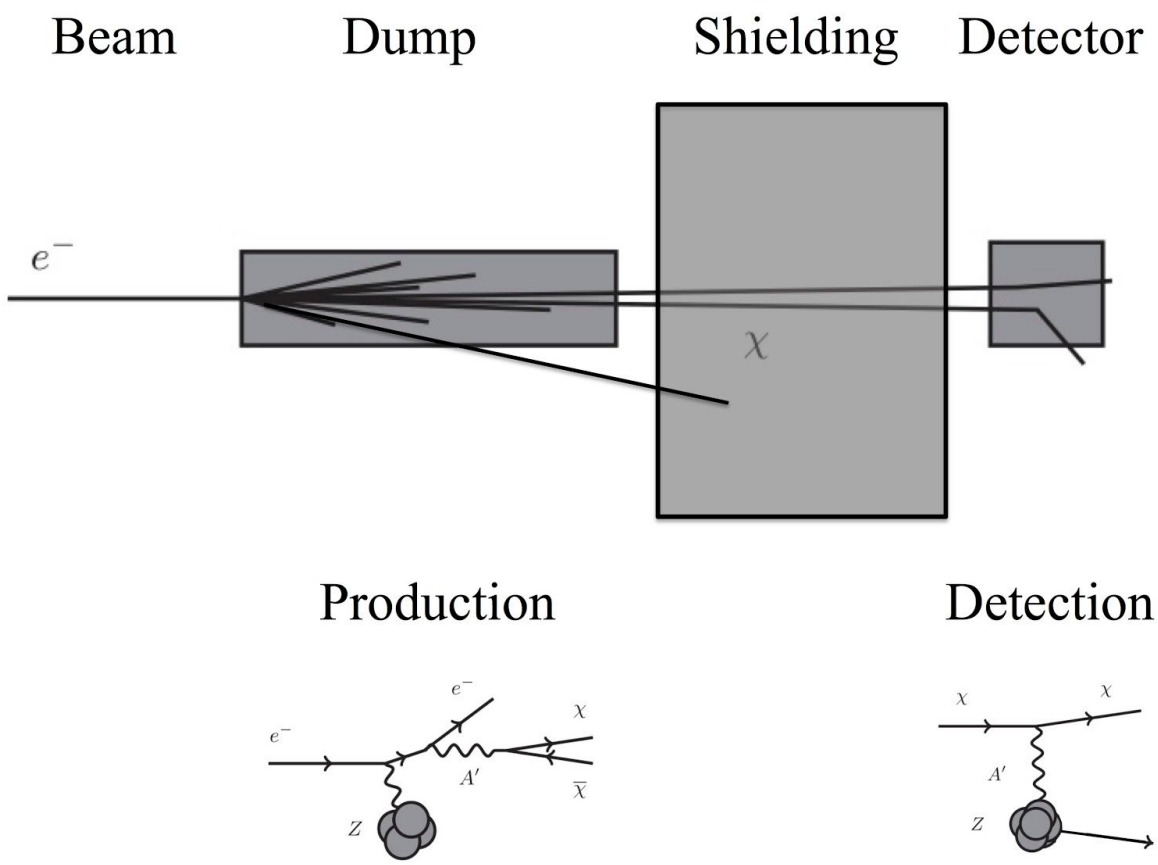

Figure 1 - A schematic, highlighting the major elements of a beam dump experiment, is shown in Figure 1. The 4 main elements of a beam dump experiment are 1) a multi-GeV electron beam, 2) an accelerator dump, 3) shielding to stop standard model particles produced in the dump and 4) a detector.

LDM particles could be produced when the electron beam interacts with the nuclei in the beam dump via the Cabibbo-Parisi radiative process producing $\chi\bar{\chi}$ pairs [4]. If the mass of the mediator *A'*, $m_{A'}$, is smaller than twice the mass of the dark matter particles, m_χ ($m_{A'} < 2m_\chi$) then the dominant production mechanism is the radiative process illustrated in Figure 1 with *A'* off-shell. In this regime, the production scales as $\sim \alpha_D \varepsilon^2 / m_\chi^2$ where α_D is the dark sector equivalent to the fine structure constant and ε governs the coupling strength between the dark sector and the normal electromagnetic sector. Both are related to couplings in the Lagrangian [4]. If $m_{A'} > 2m_\chi$ then the dominant production mechanism is the radiative production of the *A'* followed by decay into a $\chi\bar{\chi}$ pair, also illustrated in Figure 1 on the left. In this regime, the production scales as $\sim \varepsilon^2 / m_{A'}^2$.

The BDX experiment

The BDX experiment utilizes a $1m^3$-scale detector volume, located downstream of the dump of a high-intensity multi-GeV electron beam running parasitically to a scheduled experimental program. The high-energy component of beam-related backgrounds will be eliminated with specifically designed shielding made of iron and concrete blocks installed between the dump and the detector, see Figure 1. A fraction of the produced $\chi\bar{\chi}$ pair could then scatter on the electrons of the BDX detector active material. For the χ-e^- interaction, since $m_e << m_\chi$, the typical scattered electron carries GeV-scale energy producing an easily detected electromagnetic shower in the BDX calorimeter. To identify and reduce the SM background that could mimic the LDM signal, a combination of passive shielding and active vetoes will be used.

The BDX detector - The BDX detector has two main components: an electromagnetic calorimeter (Ecal) used to detect the signals produced by the interacting DM particles, and an active veto system used to reject the background. A LDM event in BDX is characterized by the presence of an electromagnetic shower in the Ecal (E>300 MeV) coupled with null activity in the Veto system.

Two hermetic plastic scintillator layers, named Inner (IV) and Outer Veto (OV), form the veto system. A layer of lead ~5 cm thick placed between the Ecal and the Vetoes is used to shield the latter from the low energy products of the electromagnetic showers escaping the Ecal. A representation of the BDX detector is shown in Figure XXX. The detector makes use of established and easy-to-handle detector technologies based on organic and inorganic scintillation detectors. The technology choices were validated with a prototype during a measurement campaign at INFN, Sezione di Catania and LNS [bdx-proposal].

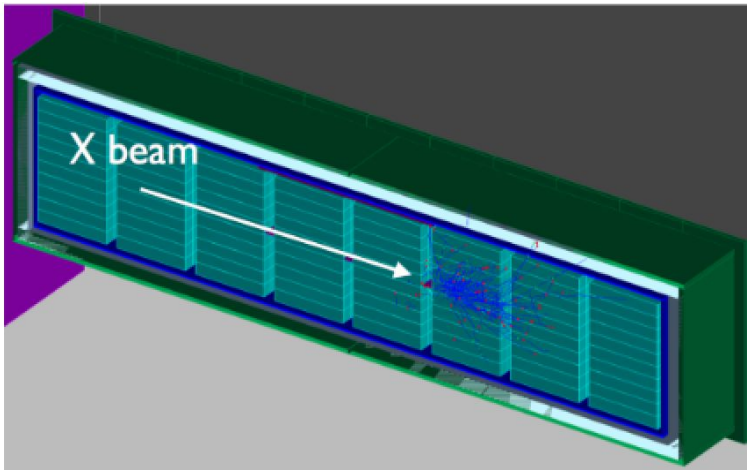

Figure XXX - The BDX detector as implemented in GEANT4. The Outer Veto is shown in green, the Inner Veto is gray and the lead vault in blue. Crystals arranged in 8 blocks of 10x10 are shown in light blue. A simulated electromagnetic shower from a χ-electron scattering in the Ecal is also shown.

Signal - The typical signal in the BDX experiment is an event with large (>300 MeV) energy deposition in the electromagnetic calorimeter, with no activity in the surrounding veto system. Depending on the specific χ interaction model, the energy deposition is due to a single scattered electron from $\chi + e^- \rightarrow \chi + e^-$ (elastic scattering), or to a (e^+/e^-) pair from the de-excitation $\chi_2 \rightarrow \chi_1 + e^+ + e^-$ (inelastic scattering). In order to evaluate the BDX sensitivity to the different LDM models, we performed a multi-step numerical calculation starting from the beam interaction with the dump to the dark beam production. The χ interaction in the detector was evaluated through a custom code, and using GEANT4-based simulation framework. The efficiency depends on the selection cuts used to identify the signal and reject backgrounds. The optimization process to determine the highest LDM sensitivity results in an efficiency of about 20%.

Background - The main beam-related backgrounds for the BDX experiment are neutrinos and very high-energy muons that penetrate through the shielding up to the detector location. These backgrounds were studied through high-statistics Monte Carlo simulations performed with the FLUKA software. The simulations included a detailed description (geometry and materials) of the Hall-A beam dump, the subsequent shielding, and the BDX detector inside the new experimental Hall. We simulated an 11 GeV electron-beam interacting with the beam-dump and propagated all particles to the location of interest sampling the flux in different locations.

A dedicated measurement campaign was performed in Spring 2018 at JLab in order to experimentally validate the framework for Monte Carlo simulation. By using the same technologies proposed for the final experiment, we demonstrated that the detector will be able to operate in the foreseen configuration, with no pile-up or other effects due to the low-energy component of the radiation field (mainly thermal neutrons produced in the dump). The muon flux was measured at different heights with respect to the nominal beam height, in two different pipes. Each experimental configuration was simulated with FLUKA (for muon production and propagation to the detector) and GEANT4 (for muon interactions with the detector). In all cases, we found excellent agreement between data and Monte Carlo, as reported in [10].

Approval - BDX was presented to the Jefferson Lab Program Advisory Committee (PACs 44, 45 and 46) and approved with the highest scientific rating in July of 2018.

The BDX-DRIFT experiment

We propose to use a low-pressure, directional TPC which, typically, have nuclear recoil thresholds, in the ~keV/amu range, and are insensitive to energetic electrons so we will only consider the nuclear elastic scattering channel in this proposal, shown on the right in Figure 1. The differential, elastic scattering cross-section for coherent detection of the dark matter particles is given, to good approximation [7], by,

$$\frac{d\sigma}{dT} = \frac{-8\pi\alpha\alpha_D\varepsilon^2 Z^2 M}{\left(m_{A'}^2 + 2MT\right)^2} \quad (1)$$

where T is the kinetic energy of the recoiling nucleus in the lab frame, α is the fine structure constant, M and Z are the mass and charge of the scattered nucleus.

The Directional Recoil Identification From Tracks (DRIFT) Detector

WIMP detectors search for ~keV/amu nuclear recoils caused by dark matter [11]. Directional WIMP detectors go a step further and attempt to measure the direction of the recoiling ions to provide a signature of WIMP interactions [12]. Low pressure gaseous detectors are preferred for this work as the recoil ranges are then long enough to be measurable [13]. For the past 20 years DRIFT has utilized *negative ion drift* to limit diffusion in ~40 Torr of gaseous CS_2 [14][15].

Negative Ion Time Projection Chamber (NITPC) Technology

A brief review relevant to this proposal is presented below.

Drifting negative ions – Invented by Dr. C. Jeff Martoff of Temple University [16], the use of negative ions to drift ionization to the readout plane reduces the diffusion of ionization to thermal values in all 3 dimensions [14][15][17] compared to electron drift [18]. This enables NITPCs to have a longer drift distance (thus a larger volume for a given area of readout) and a lower energy threshold without sacrificing directional sensitivity [19][20]. Typical ion drift velocities (5×10^{-3} cm/s[15]) are several orders of magnitude slower than typical electron drift velocities (1 cm/s [18]) making for a slow detector.

Directional Signatures – NITPCs are sensitive to the predicted sidereal modulation in WIMP direction [14]. At the location of DRIFT in the Boulby mine in England over a sidereal day (23 hours, 56 minutes cycle), the average direction of the WIMP velocity vectors relative to the detector, changes from roughly pointing south to roughly pointing down (towards the center of the Earth) [14]. The recoils caused by WIMPs will, on average, align with the direction of the average of WIMP vector vectors [21]. The robustness of this sidereal modulation as a signature for WIMPs resides in the practical impossibility of backgrounds (24 hours cycle) mimicking this effect over a year.

In practice, observing the directional signature is difficult. In DRIFT's gas mixtures, for instance, typical heavy (F and S) recoils from ~100 GeV/c^2 WIMPs are of order 1-2 mm long [22] while the fiducial volume is ~1 m^3 with 50 cm maximum drift distance and a 0.7 mm maximum thermal diffusion RMS [15]. There are two strategies for observing this directional signature. The first involves measuring recoil track range components, x, y and z. At

thresholds relevant to dark matter and with a full-sized DRIFT detector, the DRIFT collaboration has been able to observe this range component signature using neutron induced recoils [19]. The second, stronger, methodology, which involves using the differential ionization along the recoil track to identify the vector direction, or "head-tail," of the track, has also been observed [20]. As discussed below, we now operate with a mixture of CS_2 and O_2 with unique properties. Recent papers demonstrate that these signatures are preserved in these gas mixtures [23][20]. Many other groups have measured the directional signals albeit by drifting electrons and with consequently worse results [12].

Gamma/Electron/Muon Rejection – The gamma rejection capability of a NITPC relies on the well-known physics of ionizing radiation. Nuclear recoils have short tracks with high ionization density relative to Compton recoil electrons [14]. DRIFT detectors use ionization density as a trigger. By raising the ionization-density threshold it has been shown that the detector essentially never triggers (rejection factor of better than 2×10^{-7} [24]) on the high background of Compton recoil electrons, but still retains high efficiency for nuclear recoil events [25]. For the same reason NITPCs are insensitive to muons.

Cathode backgrounds - DRIFT was the first to identify radon progeny recoils (RPRs) and low energy alphas (LEAs) as a problem for gas-based directional detectors [25][26]. Both originate from alpha decays on the edges of the fiducial volume, either from the central cathode or the detectors. RPRs are caused when a radon daughter alpha decays such that the alpha is emitted into the cathode or the MWPC wires and the recoiling nucleus enters the gas, resulting in a signal nearly identical to that expected from WIMPs [25]. LEAs occur when the alpha nearly ranges out in either the central cathode or the MWPC wires and, on rare occasions, emerges with short range but ionization similar to that expected of WIMP-recoils.

O_2 Fiducialization – In 2013 Snowden-Ifft discovered that the addition of a small amount of O_2 in CS_2 or CS_2 gas mixtures creates additional anions, dubbed minority carriers [27]. These charge carriers each drift with different, discrete speeds. As with earthquake localization, the time difference between the arrival of the minority carriers is proportional to the distance travelled [27]. Thus, the distance between the detector and ionization events can be measured without a trigger. This allows for the complete elimination of backgrounds from nuclear recoils created at the edges of the fiducial volume in DRIFT [24]. In addition, knowing the drift distance, allows for precise knowledge of the point-spread function for the ionization. That, in turn, allows for deconvolution of the observed ionization and the ability to recover much of the original track's features providing for an even stronger directional signature.

Time Tested NITPC Technology – Over the past 20 years, the DRIFT collaboration has overcome many operational hurdles to achieve robust operation of our NITPC. The current detector ran nearly continuously in the Boulby mine in England for over a decade with only a modest amount of maintenance. It is still being used. As we write this proposal the detector, originally installed in 2005, is operating.

Calibration and Stable Operation – The DRIFT collaboration has gone to great lengths to understand and characterize the response of the NITPCs to nuclear recoils. Fe-55 calibrations are automatically done every 6 hours in order to monitor the gas gain to better than 1% accuracy [24]. Cf-252 neutron calibrations are done once a week and have been well matched to simulations [24].

Analysis – Finding recoils in a NITPC is like finding a needle in a haystack. As reported in [24] about 10 million events were recorded to disk over 54.7 days of live time, but no nuclear recoil events were found in the fiducial volume of the detector. All nuclear recoil events were RPRs originating from the cathode. The published limits from that experiment are shown in Figure XXX.

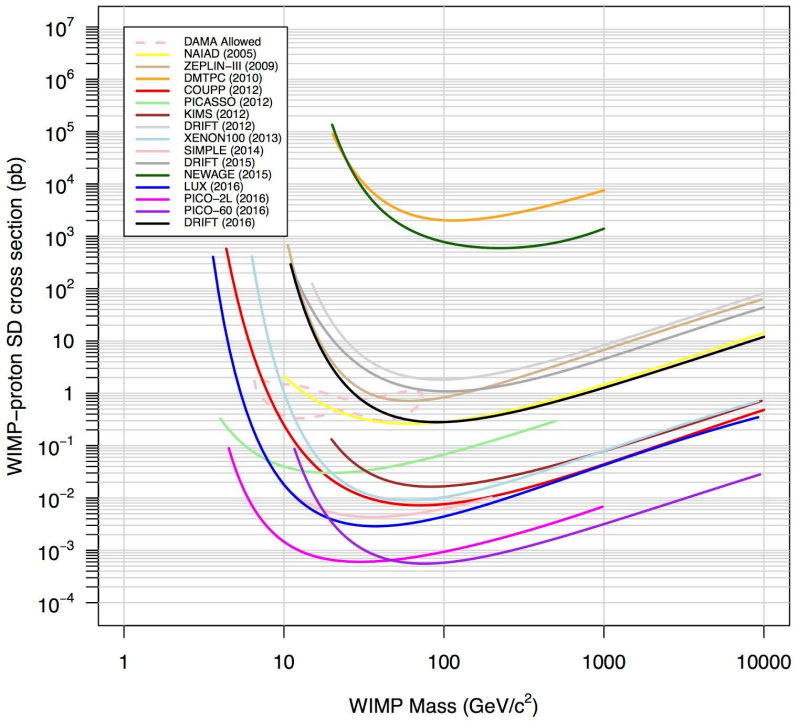

Figure XXX - Limits on WIMP dark matter from the DRIFT Collaboration in comparison with limits from other dark matter experiments. Note that the only other two directional dark matter experiments are DMTPC and NEWAGE with limits several orders of magnitude weaker than DRIFT.

To confirm that we had not inadvertently discarded nuclear recoils in the fiducial volume, the DRIFT collaboration took 45.4 days of unshielded data and found 14 events, consistent with recoils generated by ambient neutrons being emitted from the walls of the underground lab and interacting in the gas [24].

A recent unpublished analysis, shows no events in ~150 days, increasing our limit by approximately a factor of 3 from that shown in Figure XXX.

In summary, the NITPC technology developed by DRIFT over the previous several decades has unique capabilities, namely demonstrated low-threshold (*~keV/amu nuclear recoils*) and low-background (*no events observed in 150 days*) performance. We believe this technology could be usefully employed in a beam dump experiment at JLab.

BDX-DRIFT

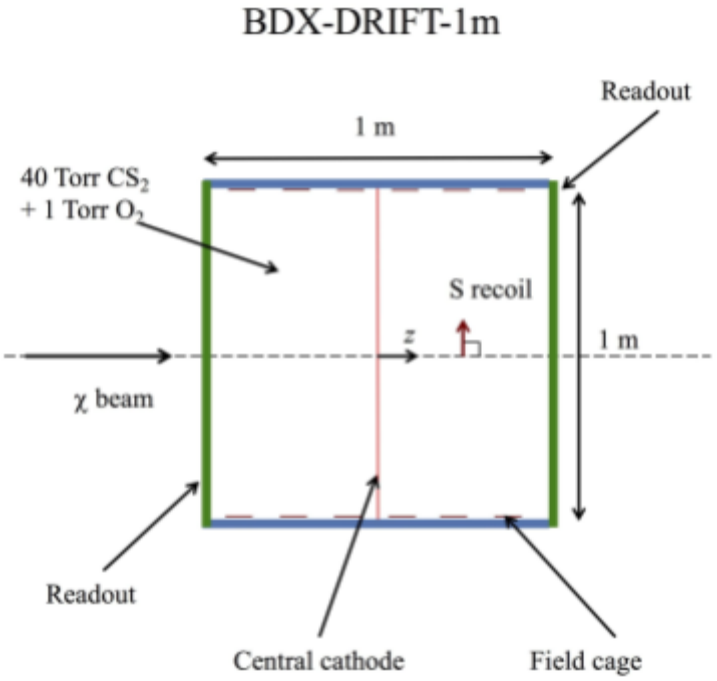

Figure XXX – A sketch of the BDX-DRIFT-1m detector. The lateral, xy, dimensions are 1 m each.

We consider a DRIFT-like detector placed behind the beam dump and explore its sensitivity and capabilities for probing the dark sector. A sketch of a BDX-DRIFT-1m module is shown in Figure XXX. The accelerator, beam dump and shielding are to the left producing a χ beam which enters from the left. The readouts on either end couple to two back to back drift volumes filled with a mixture of 40 Torr CS_2 and 1 Torr O_2 and placed into the beam, as shown. Because of the prevalence of S in the gas and the Z^2 dependence for elastic, low-energy scattering, the recoils would be predominantly S nuclei. Sulfur recoils with kinetic energies of order a few 10s of keV produced by LDM would be scattered within one degree of perpendicular to the beam line due to extremely low-momentum-transfer scattering kinematics. The signatures of LDM interactions, therefore, would be a population of events centered on the beamline, with a particular energy distribution and with ionization parallel to the detector readout planes. A BDX-DRIFT-10m detector would be made of 10 such modules aligned along the *z* dimension.

Sensitivity to the Dark Sector

For this calculation $N_e = 10^{22}$ EOT was assumed with an 11 GeV electron beam. For the dark sector parameters $\alpha_D = 0.5$,and $m_{A'} = 3m_\chi$. Dark matter flux numbers were obtained from a detailed Monte Carlo simulation done at INFN Genoa [28] including secondary scattering of the electrons in the dump. The number of detected nuclear recoil scatters was obtained by integrating Equation (1) for *T* > 20 keV. Zero background was assumed. Figure XXX shows the sensitivity (ability to exclude at 90% confidence level or greater) of a BDX-DRIFT-10m detector under these assumptions in relation to existing limits and the expectation of dark sector dark matter being a relic from the big bang. Figure XXX shows the sensitivity of a BDX-DRIFT-10m detector with the parameters as indicated.

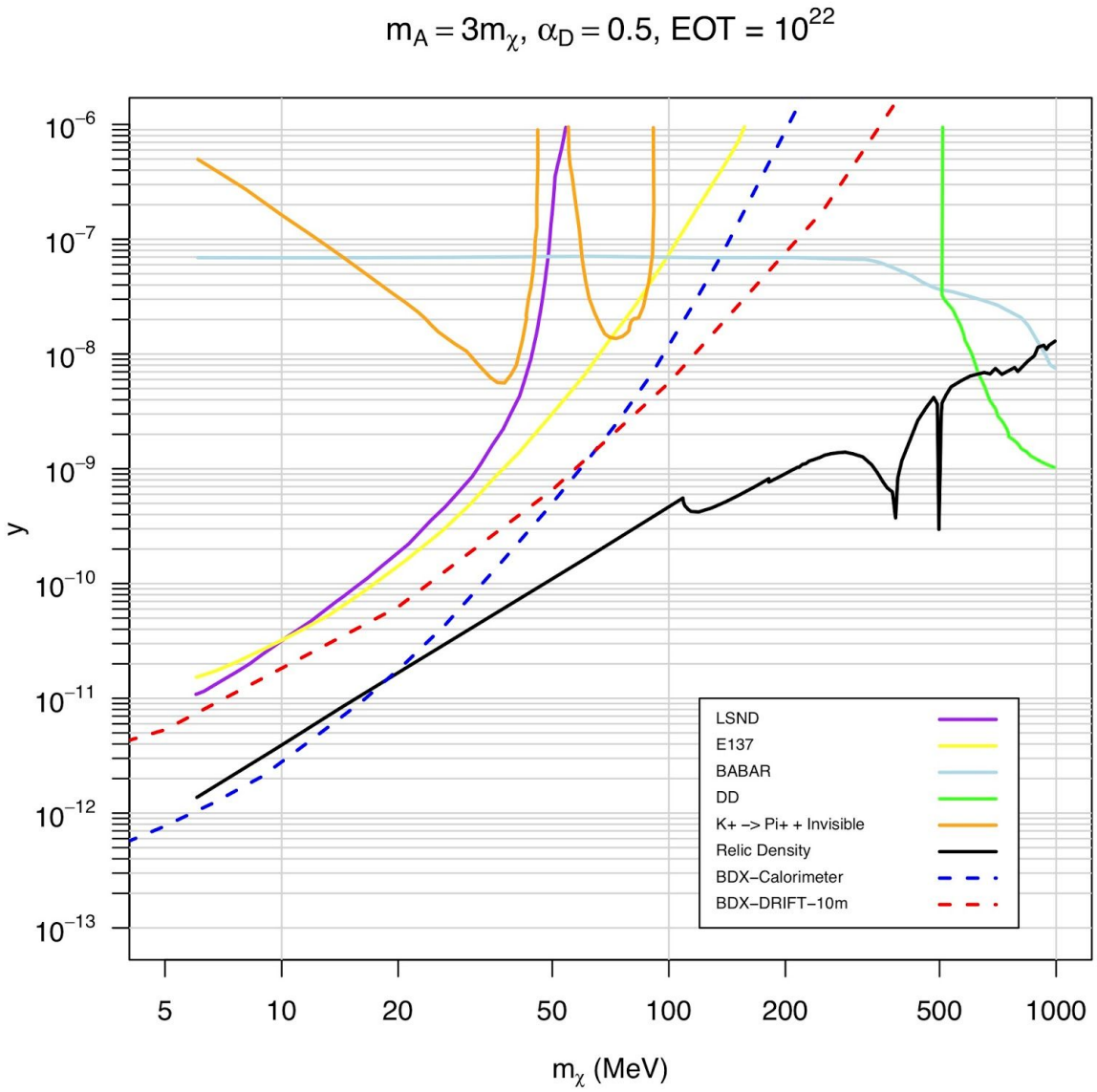

Figure XXX – Sensitivity of the BDX-DRIFT-10m detector in comparison with existing limits.

As can be seen, the limits attainable by BDX-DRIFT-10m are complementary to those of the BDX experiment. BDX-DRIFT also provides other complementarity in the exploration of other channels for detection and with different backgrounds. A detection by both detectors would be a powerful result.

Backgrounds Measured and Modeled

DRIFT has operated for decades 1 km underground in the Boulby Mine [24] and has recently demonstrated background-free operation for 150 days. In order to understand backgrounds in BDX-DRIFT at or near the surface of the Earth from cosmic rays, a series of experiments were undertaken in 2018. Data was collected above and below ground using a purpose-built, small and portable DRIFT detector called BDX-DRIFT-0.3m and the results compared to GEANT simulations.

BDX-DRIFT-0.3m

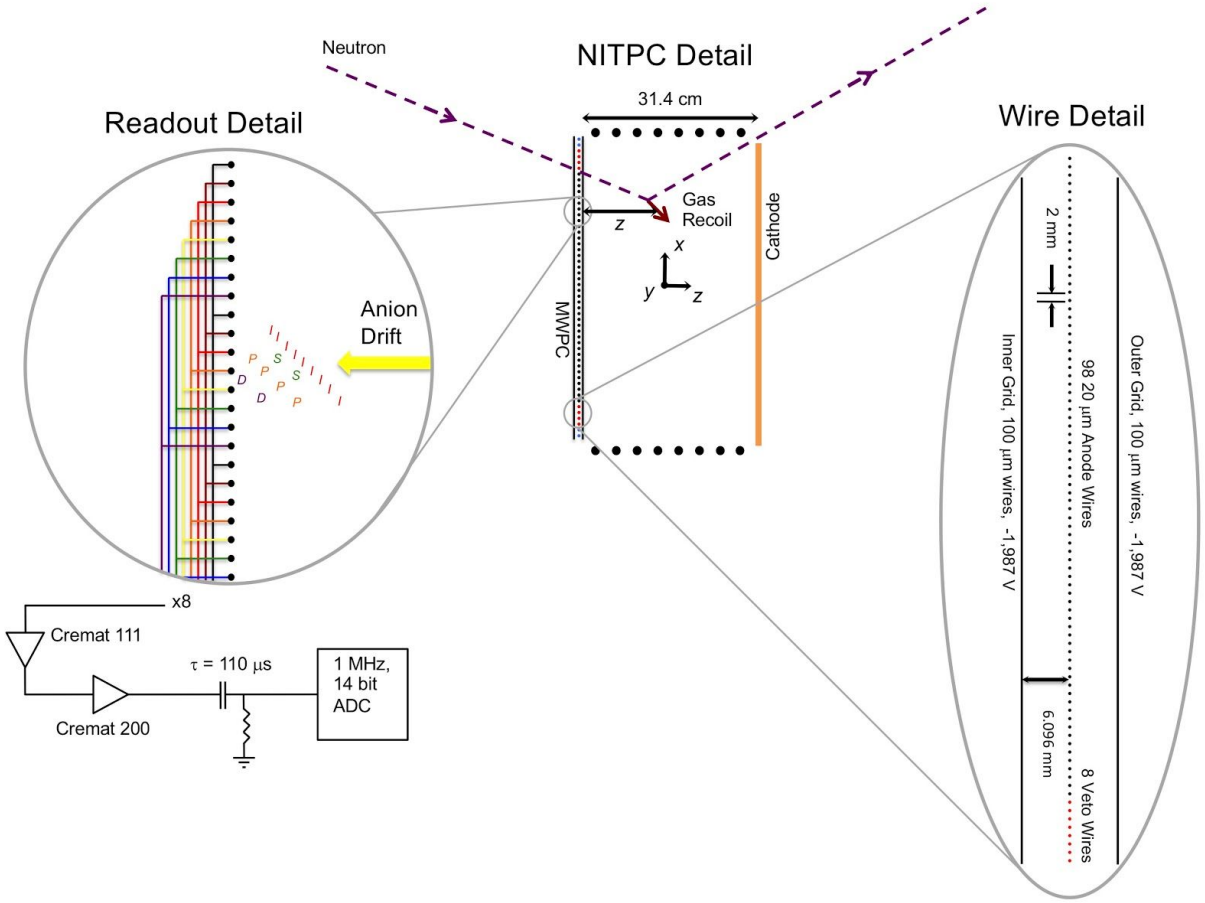

Figure XXX - The BDX-DRIFT-0.3m NITPC Detail shows a schematic of the NITPC, as viewed from above. It is composed of an MWPC, a central cathode and a field cage. A neutron is shown interacting in the gas inside the fiducial volume of the detector. The Readout Detail shows the separation of the minority carriers, labeled D, P, S on the way to the readout allowing the distance *z* from the MWPC to be determined. The anode and grid wires of the detector are grouped into 8 readout lines and read out as shown and discussed in the text. The Wire Detail shows details of the MWPCs.

For all of the runs, the cathode, see Figure XXX, was held at a voltage of -17.7 kV. The inner grid planes of the MWPCs were located 31.4 cm away from the central cathode (in the *z* dimension, see Fig. 1) and were biased at -1.987 kV. Thirteen stainless steel tubes with ¼" diameter surrounded the fiducial region with stepped voltages to provide a uniform drift field of 500.8 V/cm drift field. The entire vacuum vessel, described below, including the fiducial volume was filled with a mixture of 40 Torr CS_2 + 1 Torr O_2.

Figure XXX - The BDX-DRIFT-0.3m NITPC on the lab bench. The MWPC is towards the front. The ¼" field cage rings and connecting resistors are seen through the MWPC wires (not visible in photo). At the back is the Al cathode.

The MWPCs, see Fig. 1 – Wire Detail, were made up of a central, grounded, anode plane of 114 20-μm-diameter stainless steel wires on a 2 mm pitch (measuring the *x* extent of the events), sandwiched between two perpendicular, grid planes of 114 100-μm-diameter wires at -1.987 kV, again on a 2 mm pitch (measuring, using induced pulses, the *y* extent of the events) and separated by 6.096 mm from the anode plane. There are 98 anode and grid wires that form the lateral (*xy*) dimensions of the fiducial region giving a square, fiducial area of 384 cm^2. Eight of the remaining wires on each side formed an anode or grid veto.

For both anode and grid, every 8^{th} wire in the fiducial area (98 wires) was grouped together, providing 16 mm of readout per event in both *x* and *y*, see Figure XXX - Readout Detail. This was sufficient to contain the ~few mm recoils of interest. After a gas gain of ~1,100 all signals were pre-amplified inside the vacuum vessel by Cremat CR-111 preamplifiers, then amplified by Cremat CR-200 shaping amplifiers (4 μs shaping time) outside of the vacuum vessel.

Finally, the signals passed through a high-pass filter with time constant 110 μs and were digitized by 14-bit National Instruments PXI-6133 ADCs at sampling rate of 1 MHz with 0.152 mV resolution. The DAQ was triggered to read out all channels when any one of the anode signals rose above a threshold of 20 mV on a box-car-smoothed signals over 18 μs. Both pre- and post-trigger data were recorded (2 ms and 9 ms respectively). Anode and grid veto signals were read out separately for each MWPC. With the grouping scheme described above, only 18 channels were needed to read out the entire detector.

Moving outward, a 6 mm thick acrylic shield prevented discharge to the grounded vacuum vessel. A solenoid-activated Fe-55 sources periodically irradiated the detector with 5.9 keV X-rays to calibrate the gas gain. A cylindrical stainless-steel vacuum vessel with interior dimensions ~2 ft by ~3 ft and mounted on wheels surrounded the entire apparatus, see Figure XXX.

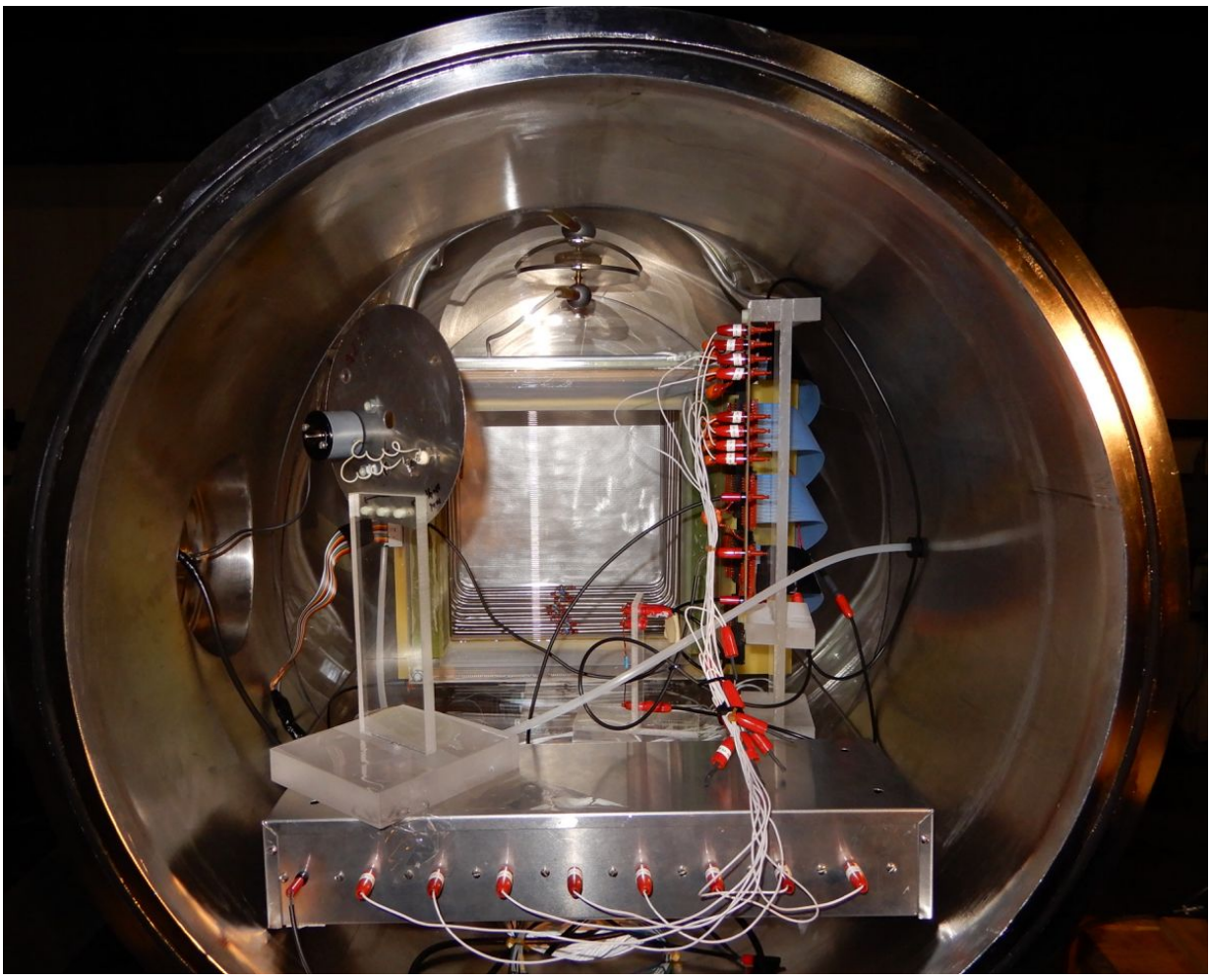

Figure XXX - The BDX-DRIFT-0.3m NITPC inside the vacuum vessel below the HHV feedthrough at the back. The Fe-55 source is seen on the left at the front. The cathode readouts are shown on the bottom and right.

Finally, a custom-built gas system mixed evaporated CS_2 with O_2 to provide the requisite 40 Torr CS_2 + 1 Torr O_2 gas mixture to the vacuum vessel. After flowing through the vacuum vessel, the bulk of the CS_2 was captured by pumping it to the bottom of a stainless-steel waste canister where it liquefied under several centimeters of water. Any remaining CS_2 was captured in a carbon trap. A browser-based control system enabled remote control of the detector and also provided system feedback on a number of channels (pressure, voltage, current etc.) at a rate of 1 sample every 4 seconds. As can be seen in Figure XXX the entire system (vacuum vessel, gas system, electronics rack etc.) was on wheels to provide portability.

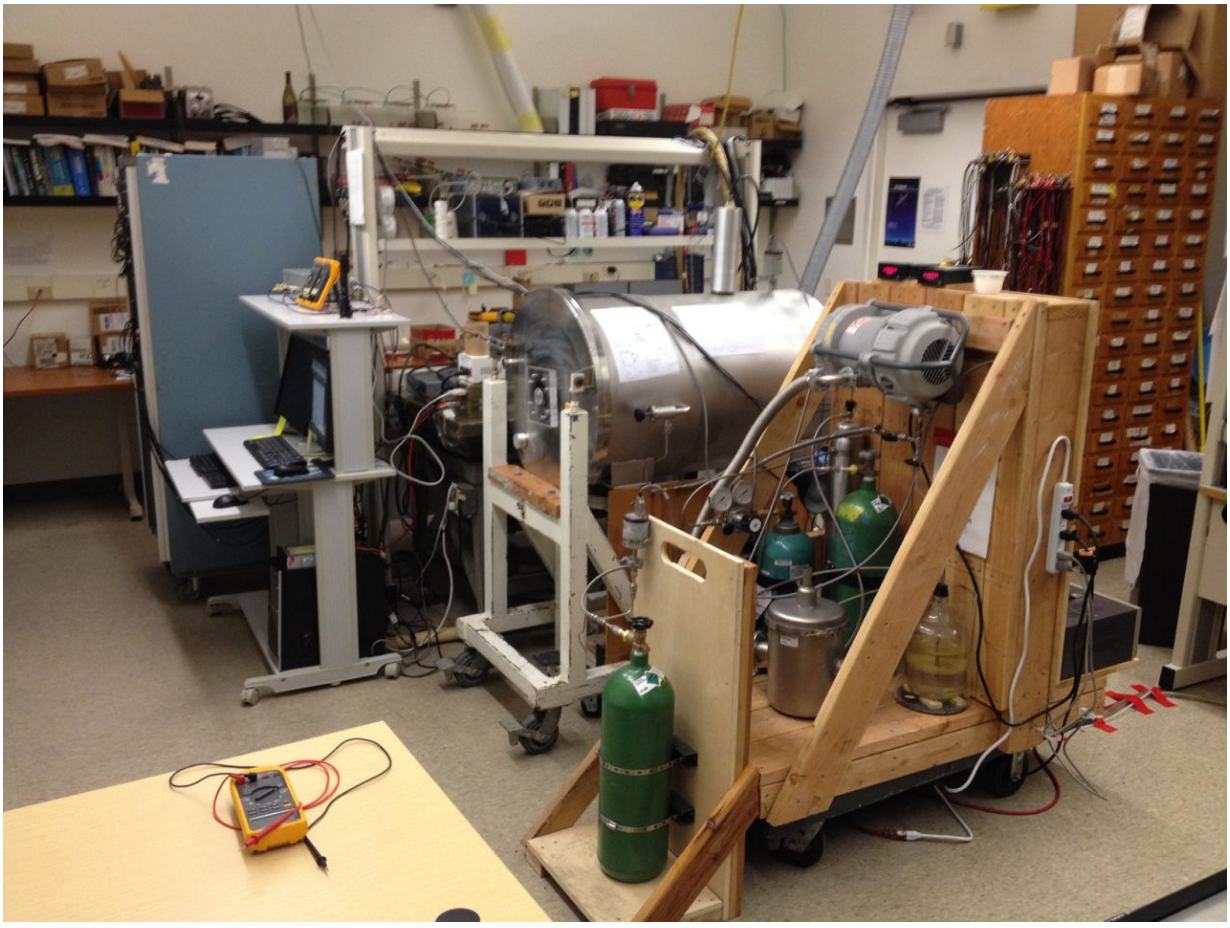

Figure XXX - The BDX-DRIFT-0.3m detector. In the foreground is the gas mix system. Behind it is the vacuum vessel. Readout electronics is shown on the left.

End Station A (ESA) SLAC

During the summer of 2018 the Occidental group traveled to the Stanford Linear Accelerator facility to conduct a series of experiments. One experiment was done in the ESTB facility, formerly known as End Station A (ESA). As shown in Figure XXX this facility is a large concrete building with a parasitic beam line entering it. During the accelerator run, 3.8 live-time days of background data were collected.

a) b)

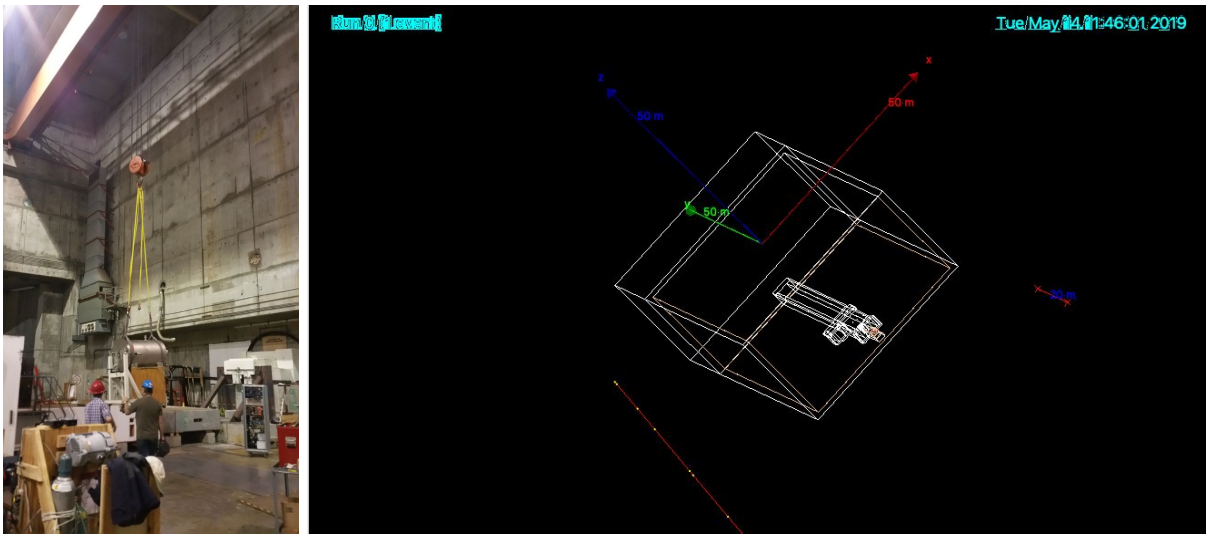

Figure XXX - a) Inside ESA at SLAC with the detector being installed. (b) A GEANT simulation model of SLAC's ESA facility. The facility is a large concrete structure with a beam line entering one end and traveling almost the entire length. The detector was located near this end shown, roughly, in brown on the diagram above.

Tunnel to End Station B (ESB) SLAC

After the accelerator run was completed, the BDX-DRIFT-0.3m detector was moved to the tunnel leading to End Station B (ESB). This tunnel is buried beneath 20' of dirt, very similar to the overburden of the proposed beam dump facility at JLab. Figure XXX shows the geometry. 34.7 days of live-time data were collected in the ESB tunnel during the late summer and early fall of 2018.

a) b)

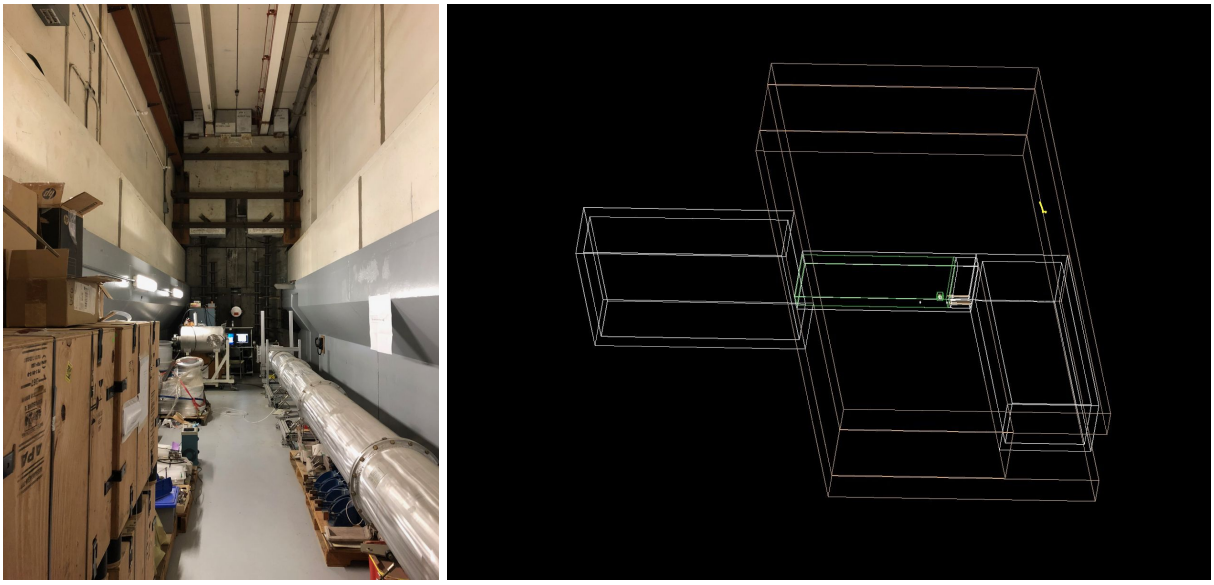

Figure XXX - a) A picture of the inside of the ESB tunnel. The detector is shown in the back left just in front of the shielding separating the ESB tunnel with the beam switchyard. b) A GEANT simulation model of SLAC's ESB tunnel. The facility a tall, narrow tunnel, highlighted in green, which use to bring the beam to the ESB facility shown on the left above. The detector is shown as a small green cube on the right end of this tunnel. To the right of the detector is a concrete shielding which separates the tunnel from the beam switchyard to the right.

The analysis of DRIFT data, particularly with the advent of minority carriers, is complex. A full description is provided here [24]. Briefly, each of the 18 channels is analyzed separately and 17 parameters are generated per channel. Cuts are placed on these parameters to winnow the data. At that point a machine-learning algorithm, trained on Cf-252 neutron recoil data, selects events as the final cut. An example of an event from a neutron calibration run is shown in Figure XXX. The most important parameters to emerge from this analysis measurements of the amount of ionization *NIPs* (for number of ion pairs) and the distance to the readout plane, *z*.

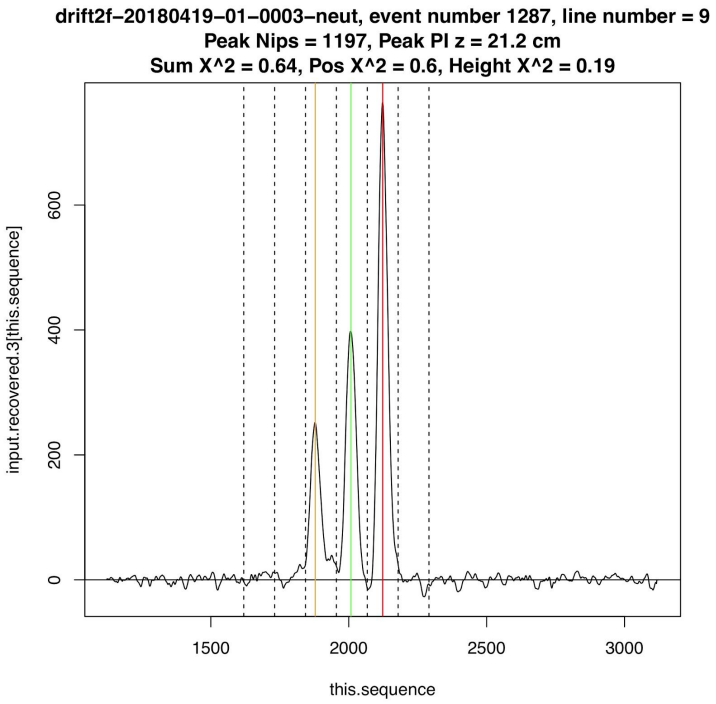

Figure XXX - An example event from one of the Cf-252 neutron calibration runs. The red line shows the location of the I-peak. The gold and green lines show the location of the minority peaks. For this event the D peak is not visible. The vertical dashed lines show the breaks for evaluating the individual peaks including pre and post veto bins.

Figure XXX below shows *NIPs* vs *z* data taken during a Cf-252 calibration run and a background run..

a) b)

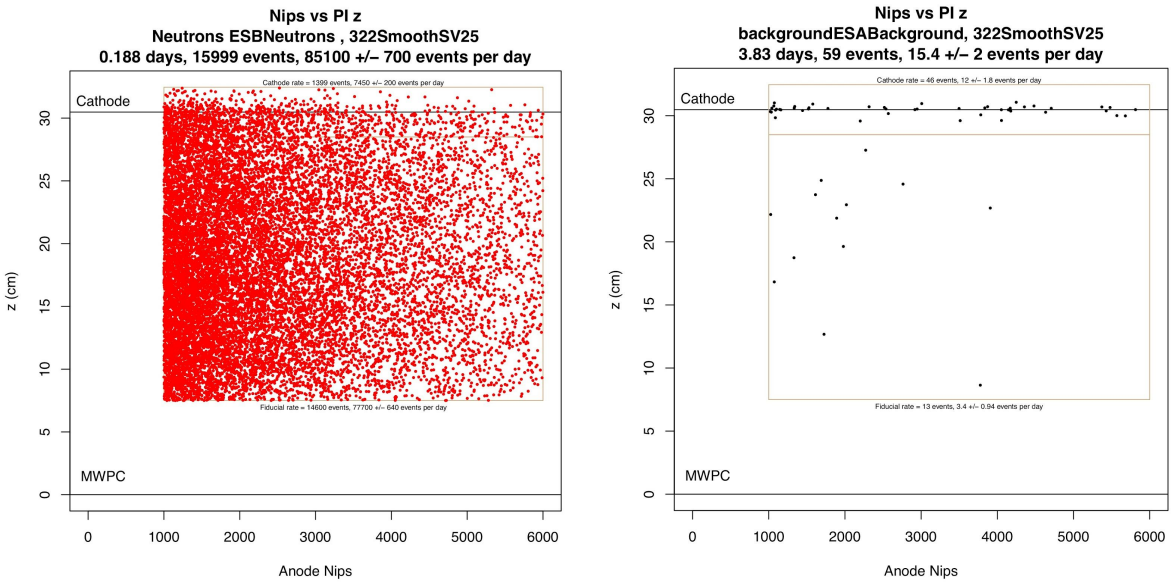

Figure XXX -a) *NIPs* vs *z* data taken during a ESB Cf-252 neutron calibration run. Overlapping peaks for small drift distances limit analyzable recoils to $z > 7.5$ cm. b) *NIPs* vs *z* data taken during a ESA background run. The events clustered around the cathode are RPR events. In order to exclude RPRs from the final data set, recoils are required to have $z < 28.5$ cm. This then defines a fiducial region in *z* ($7.5 < z < 28.5$ cm), 21 cm long. Additionally for this analysis data were required to have between 1000 and 6000 *NIPs*. These parameters define BDX-DRIFT-0.3m's fiducial region shown as the lower tan box here.

Overlapping peaks for small drift distances limit analyzable recoils to $z > 7.5$ cm, see Figure XXX a). The events clustered around the cathode during the background run, Figure XXX b), are RPR events. In order to exclude RPRs from the final data set, recoils are required have $z < 28.5$ cm. This then defines a fiducial region in *z* ($7.5 < z < 28.5$ cm), 21 cm long. Additionally for this analysis data were required to have between 1000 and 6000 *NIPs*. These parameters define BDX-DRIFT-0.3m's fiducial region shown as the lower tan box here in Figure XXX b).

The results are presented in Table 1, last column. As can be seen, a rate of events passing all of the cuts near the surface, ESA, is only a few per day. During these runs, cosmic ray muons passed through the fiducial volume of the detector at a rate of 350,000 per day showing insensitivity to them. As discussed above, this is is due to low ionization density of the cosmic rays in the low pressure gas and the relatively high threshold placed on ionization density. Moving the detector under 20' of dirt, in the ESB tunnel, resulted in a factor of ~30 reduction in the observed nuclear recoil rate.

Table 1 - Summary of Predicted (GEANT + Efficiency Map) and Experimental Results

Location	Cosmic-ray particle type	Predicted Rates (day^{-1})	Experimental Rates (day^{-1})

SLAC ESA	neutron	3.20 +/- 0.09	3.8 +/- 0.1	3.4 +/- 0.9
	muon	0.38 +/- 0.01		
	proton	0.17 +/- 0.02		
SLAC ESB	muon	0.13 +/- 0.01	0.14 +/- 0.01	0.23 +/- 0.08
	neutron	0.0037 +/- 0.0009		
	proton	0.00016 +/- 0.00008		

In order to understand these results detailed GEANT simulations were done for each of the locations. Three cosmic ray sources (muon, neutron and proton) were considered. The CRY [29] library was used to model the source spectra at the surface of the earth. Nuclear C, S and O recoil positions and energies were recorded in the fiducial volume of a simulated BDX-DRIFT-0.3m detector. Recoil energies were converted into *NIPs* utilizing [24].

In order to take into account detector and analysis efficiencies, neutron calibration data and a detailed GEANT Monte Carlo were used to generate an efficiency map, see Figure XXX.

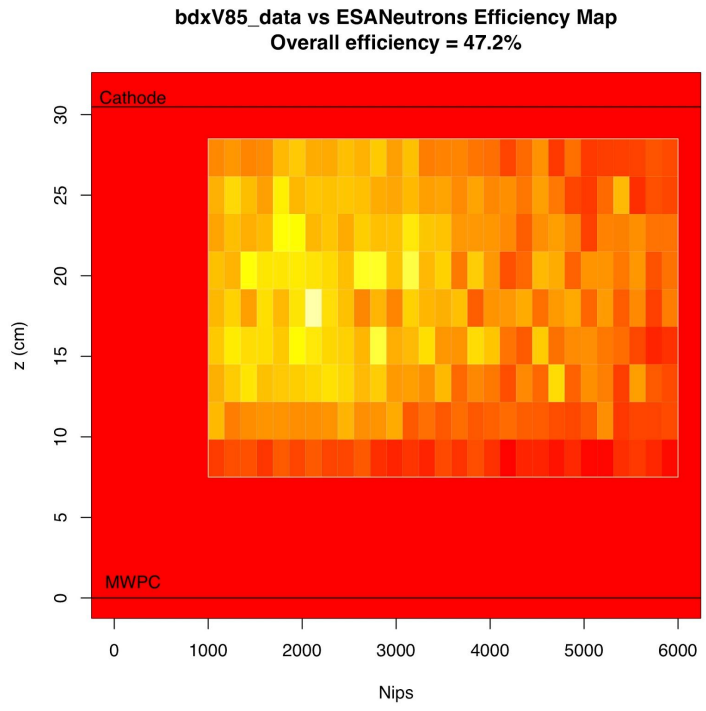

Figure XXX - The efficiency map for the ESA run. Each box shows the efficiency for detection at that location in the fiducial volume.

The details of the efficiency map are discussed in [24]. Briefly, the efficiency map is obtained by dividing, cell by cell, the observed number of events by the number of events predicted by GEANT at that location. Once in hand, the efficiency map allows for the prediction of observed recoils from predicted recoils with all systematics from detector and analysis effects taken into account. Overall the efficiency for detecting events for this analysis was about 50% in this fiducial region. This is expected to improve in the future.

Efficiency maps were made for both locations (ESA and ESB) and, despite the potential for several systematics to enter the calculation, they agreed well with each other.

Recoil *z* positions vs *NIPs* maps from GEANT were multiplied by efficiency maps, see Figure XXX, to obtain predicted rates. These numbers are shown in columns 2-4 in Table 1. As can be seen, cosmic ray neutrons dominate for near the surface while muon induced neutron recoils dominate underground.

The SLAC ESA comparison shows good agreement between prediction and data. The SLAC ESB results are in statistical agreement but the error bars are large due to paucity of nuclear recoil data from the underground location. Note that the predicted result for the ESB tunnel was affected by a complex environment. For instance, more than half of the muon contribution to the SLAC ESB predicted rate came from muon induced neutrons from various metal objects in the tunnel, see Figure XXX a) that had to be included in order to obtain an accurate result. The agreement between predicted and experimental results suggest that the detector is sensitive only to nuclear recoils, that the efficiency map is an accurate reflection of detector inefficiencies and that GEANT does a reasonable job at modeling nuclear recoils inside of BDX-DRIFT under varying conditions.

Cosmic Ray Backgrounds

With a benchmarked simulation protocol in hand we have performed GEANT [30] simulations of a BDX-DRIFT-10m detector surrounded by a 7 mm thick Al vacuum vessel in turn surrounded by 0.75 m of shielding, under a 20’ overburden of earth and exposed to cosmic rays on the surface. Nuclear recoils above a 20 keV (S equivalent) threshold occur at a rate of ~1.5 events per day within 10 cm of the beam line, the expected beam profile for the lowest mass LDM particle, see Figure XXX below. With an expected beam-time of ~285 days to achieve 10^{22} EOT we would expect ~425 beam-unrelated background events within 10 cm of the beam line for the entire exposure, an unacceptable level of background.

Small signals (~1,000 anions) and long and slow ion drift (10 ms maximum drift time) make it unlikely that timing resolution better than ~10 μs can be achieved [15], far too long for a bunch-timing-veto at JLab. For this reason, a neutron-recoil veto is required.

We are considering a muon/neutron veto composed of B or Gd doped water or liquid scintillator surrounding the vacuum vessel [31][32][33]. For simulations presented in this proposal we model a 75 cm thick veto composed of Gd doped liquid scintillator. A detailed study of such a veto concluded that 99% of neutrons can be vetoed [33]. Furthermore 90% of the neutron-recoil background is due to muon-induced-neutrons created *inside* the neutron veto/shielding. These events will be easily vetoed by the energy deposited by the muon as it traverses the neutron veto. Thus we expect >99.9% veto efficiency based on these initial estimates, see R&D section for further discussion of this topic.

The inclusion of a neutron recoil veto reduces our accepted events to less than 0.4 events within 10 cm of the beam line for the entire 10^{22} EOT exposure.

Note that the current conceptual drawings for the underground BDX experimental hall at JLab show large vertical shafts for equipment and personnel access reducing overburden for the experimental area, see Figure XXX. We have simulated the increase in cosmic backgrounds in BDX-DRIFT due to this reduction in overburden and found they would increase by roughly a factor of five. Several cost effective measures are being explored to reduce this background but in the worst case backgrounds would be ~2.0 events within 10 cm of the beam line for the entire 10^{22} EOT exposure. Beam-off time measurements can be used to statistically reduce this background. As discussed below we can also utilize powerful event signatures to allow further background suppression and signal detection.

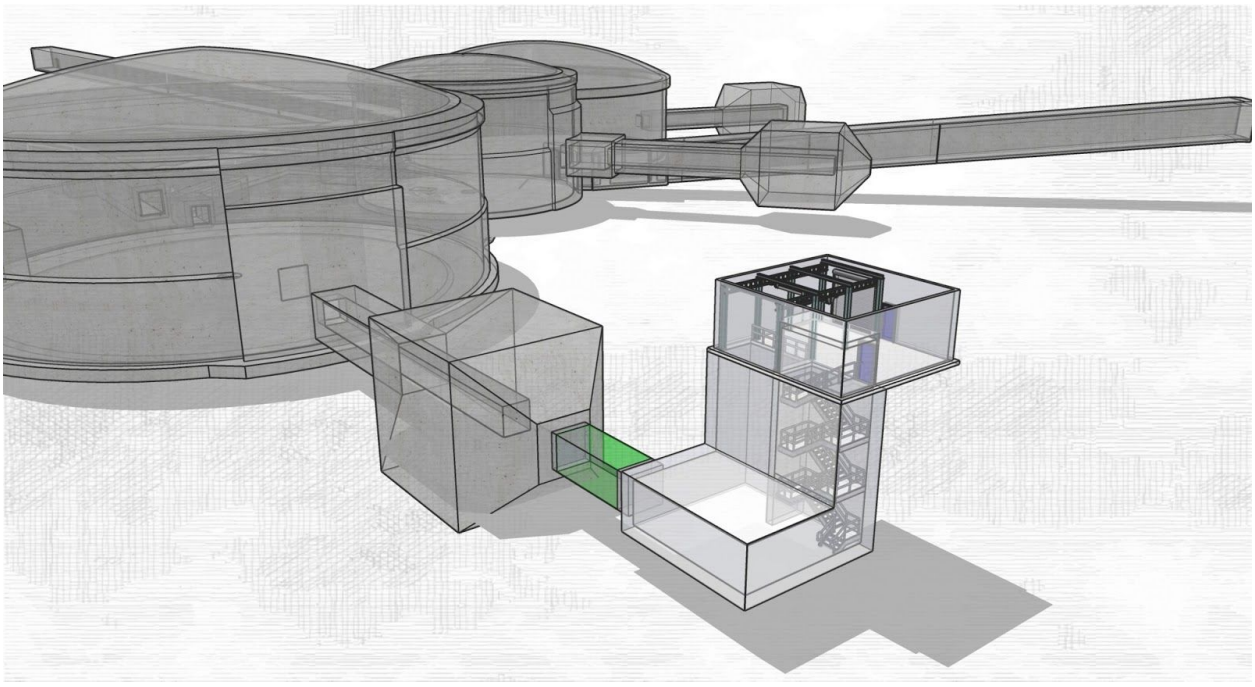

Figure XXX - A conceptual drawing of the BDX facility at JLab.

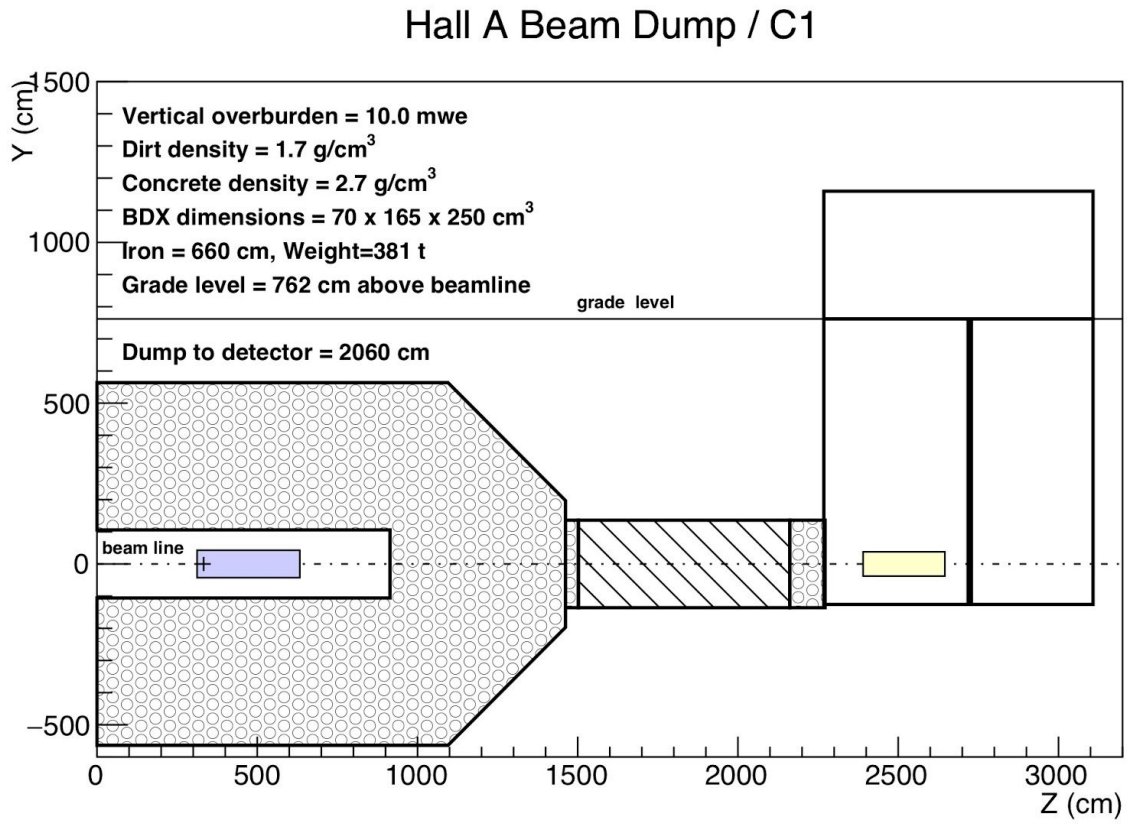

Figure XXX - Cross-section of the BDX facility at JLab with dimensions.

Beam-Related Backgrounds

Neutrinos

Using our GEANT simulation of the BDX facility at JLab, see Figure XXX, we estimate that 5×10^{16} neutrinos will pass through the fiducial volume of the BDX-DRIFT-10m detector over the course of a 10^{22} EOT exposure. With a typical coherent, elastic, neutrino-nucleus scattering cross-section of order ~10^{-39} cm^2 [34] we expect only 0.2 coherent scattering events from neutrinos for the proposed run in the entire BDX-DRIFT-10m detector. Thus we would expect 0.007 events from coherent neutrino nucleus scattering within 10 cm of the beam line for the entire exposure.

Muons

In order to estimate muon backgrounds related to an exposure of 10^{22} EOT we took a staged approach based on a benchmarked production model and conservative estimates at every turn.

Stage I - Following the C2 conditional approval of the BDX experiment at JLab, the BDX collaboration performed several experiments to benchmark the production and propagation of muons produced in the Hall A beam dump. These results have now been published [10] and show good agreement with GEANT and FLUKA simulations.

Not reported in that work but relevant for this calculation was a muon production model discussed in [35]. The aim of this latter work was to probe leptophilic dark sectors utilizing muons created at electron beam-dump facilities. The authors are members of the BDX collaboration. In that work the authors present a model of muon production for an 11 GeV electron beam impinging on an Al beam dump identical to the Hall A beam dump.

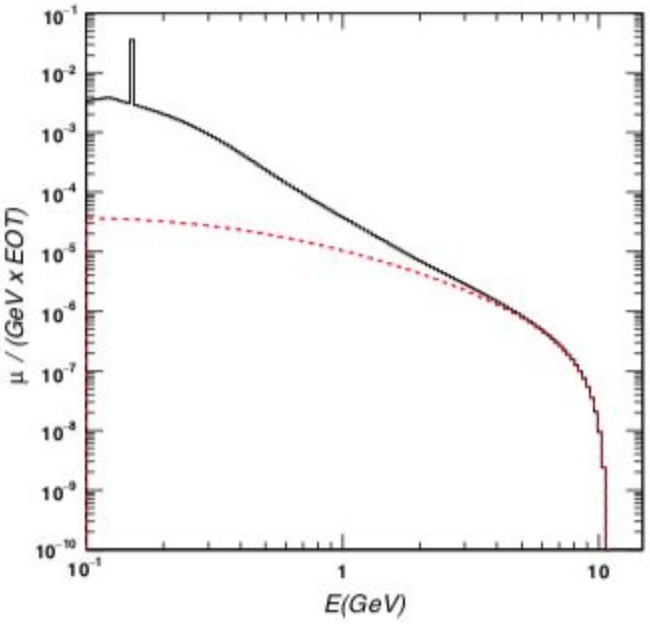

Figure XXX - "The differential muons yield per EOT for an 11 GeV e- beam impinging on a thick aluminum and water target, as a function of the muon kinetic energy. The continuous black curve refers to all produced muons, while the dashed red curve refers only to pair-produced muons. The peak in the full distribution at E = 152 MeV is due to the kaon decay-at-rest process, $K \rightarrow \mu\nu_{\mu}$." [35]

This muon production model with muon range data supplied by [36] was used to predict the rate of muons entering the detector at the Well 1 position referenced in [10]. The results are in agreement with the muon production model to within 5%, validating the model. We therefore start with this model. Muons less than 3 GeV will not penetrate the concrete shielding surrounding the Hall A dump. Integrating the spectrum shown in Figure XXX from 3 GeV to the maximum energy we find that each one of these muons corresponds to 2.1×10^5 EOT.

Stage II - The spectrum from 3 GeV and above was entered into GEANT and the muons were fired at the start of the beam-dump, where we assume most of them would be created. 4.7×10^7 muons were simulated. Most of these muons range out in the concrete surrounding the beam dump or in the iron shielding shown in Figure XXX, but 183 were found to exit the concrete portion of the beam dump or the iron shielding into the dirt. These are shown in Figure XXX.

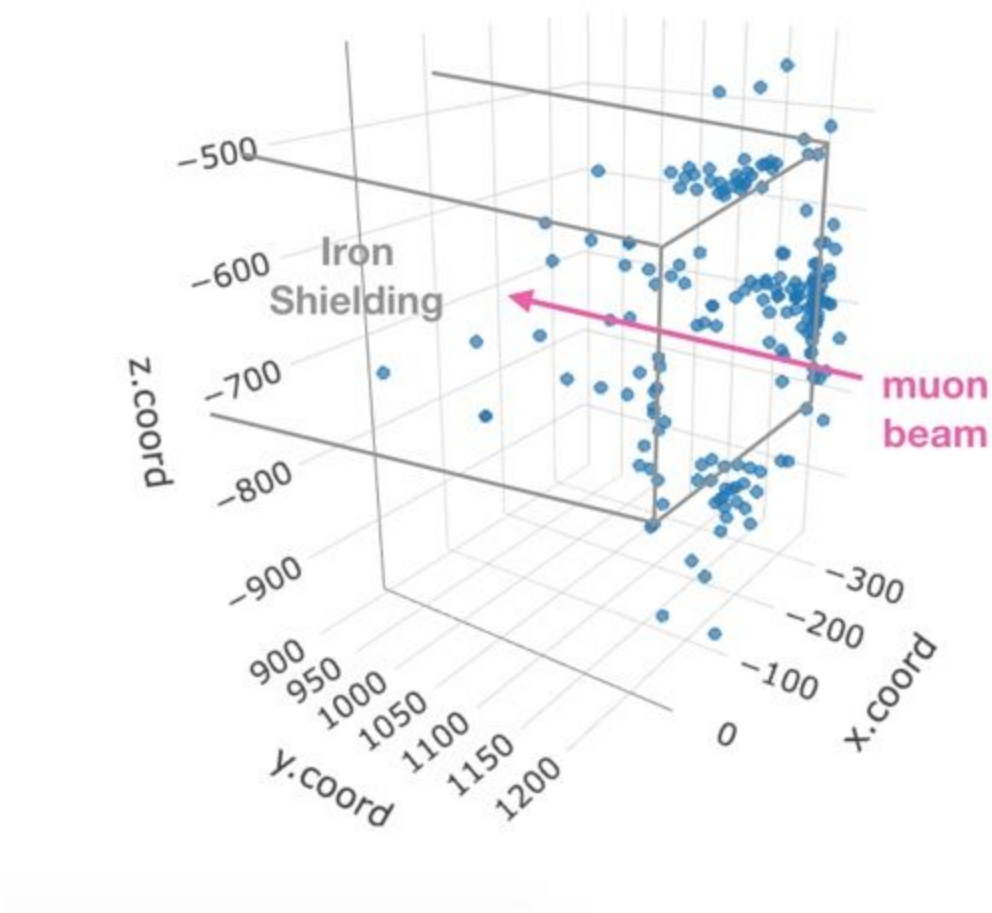

Figure XXX - This shows where muons created in the beam dump, to the right in this figure, exit the concrete shielding surrounding the beam dump and iron shielding and enter the dirt.

Most exit at the juncture between the concrete shielding and the Fe shielding. From above we obtain 1 muon exiting into the dirt for every 4×10^{10} EOT.

Stage III - For this stage of the simulation we fired 7.4×10^{8} muons from the juncture between the concrete shielding and the Fe shielding but, to be conservative, we gave each the maximum energy possible. This was calculated assuming that muons generated at the beginning of the beam dump, in fact missed it, losing energy only in the concrete shielding. Many of these muons were able, because of the generous assumption on the energy, to penetrate the remaining dirt and scatter into the experimental hall, shown in Figure XXX. We recorded 11 nuclear recoils in a single BDX-DRIFT-1m detector with 25× the nominal 40 Torr pressure. 4 of these recoils were above threshold. We are therefore predicting, conservatively, a background of ~400 events spread over the entire volume during the full exposure of 10^{22} EOT. All of the observed events were created by muons after entering the veto and so would have been vetoed, as discussed above. We expect these events to be vetoed as discussed above for beam-unrelated backgrounds reducing beam-related

backgrounds from muons to ~0.01 events within 10 cm of the beam line for the entire exposure.

Moving to a larger configuration of iron shielding, configurations B or C (shown below in Figure XXX), discussed in the PAC 46 update would entirely eliminate this beam-related background.

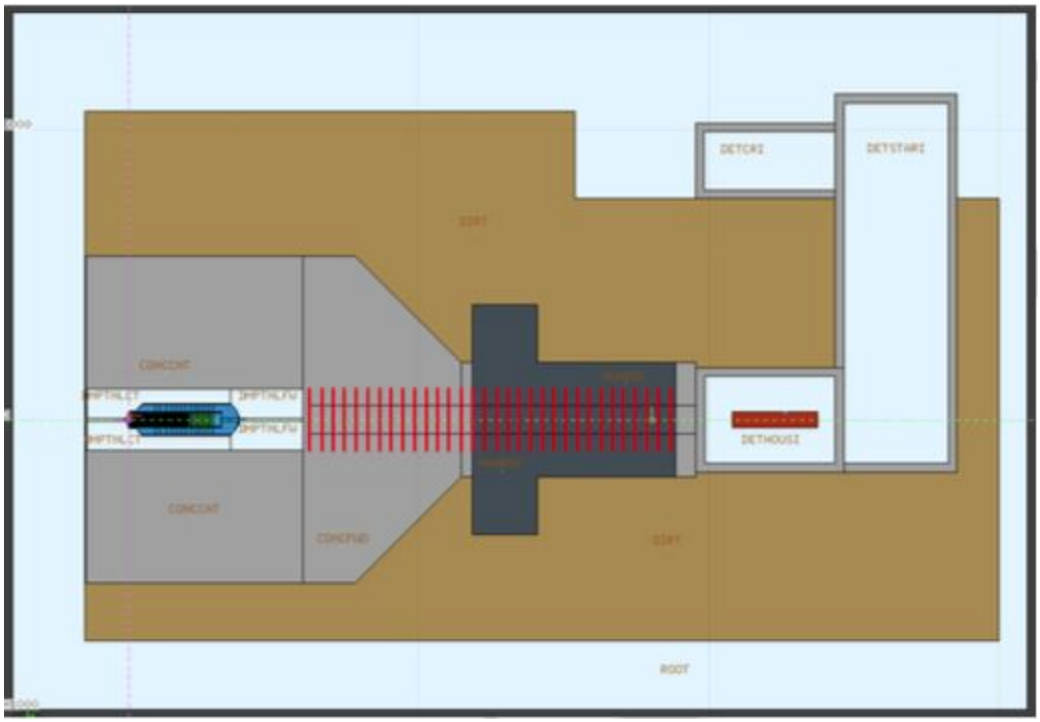

Figure XXX - Larger iron shielding structure discussed in the PAC 46 update by the BDX collaboration. This is one possibility for removing beam related muon backgrounds discussed in the text.

Neutrons

In order to estimate neutron backgrounds related to an exposure of 10^{22} EOT we, again, took a staged, conservative approach based on experimental data.

Stage I - We begin this calculation with measurements of neutrons emanating a beam dump at SLAC [37], see Figure XXX,

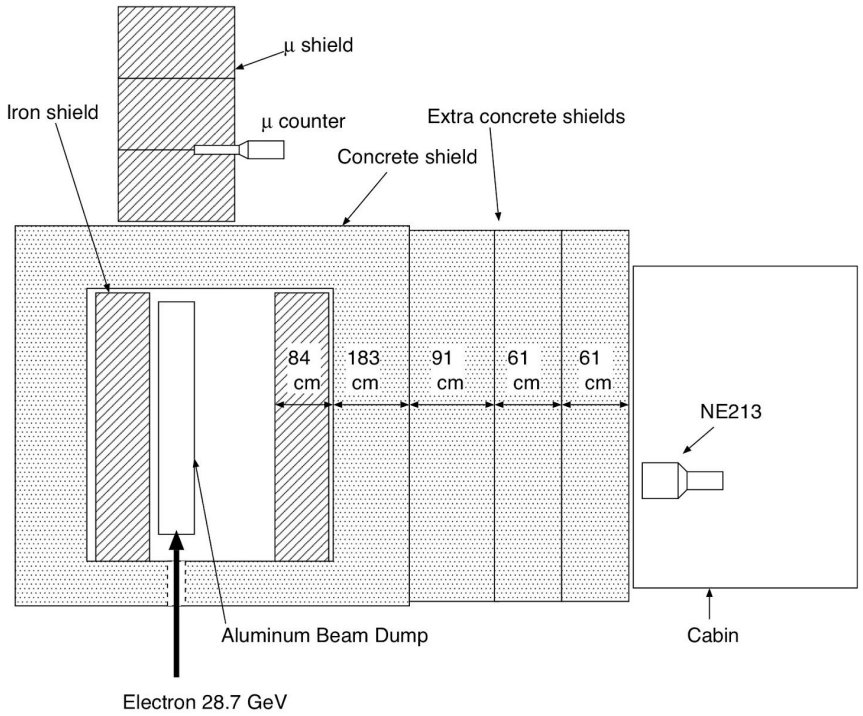

Figure XXX - The experimental setup for measurement of neutrons emanating from a beam dump at SLAC [37].

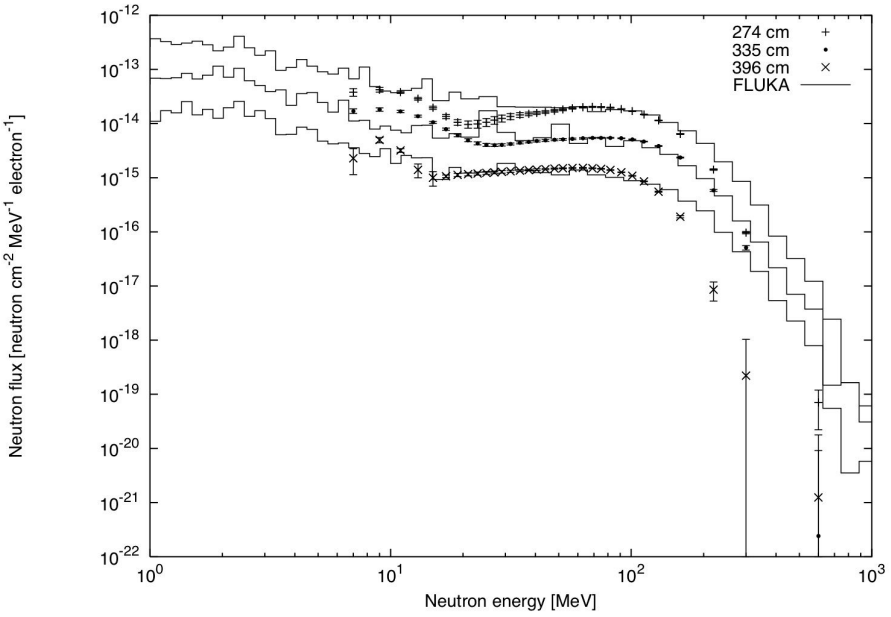

Figure XXX - The measured energy spectrum. For this calculation we used the 396 cm data.

Note that the beam energy is 28.7 GeV/11 GeV = 2.6× the beam energy expected for the JLab exposure. To account for the iron shield, not present at JLab, we rely on simulations of

neutrons through iron shielding [29] which suggests a simple factor of ×40 reduction in neutron flux with no change in the shape of the spectrum, see also Figure XXX. We boost the production of neutrons by ~40/2.6 = 15 to make a first-order correction for these differences.

The energy spectrum we utilized was that of the Fluka simulation shown in Figure XXX b) for the 396 cm data which is generally higher than the data, so, again, we make a conservative approximation. Integrating the spectrum from 1 MeV to 1 GeV we find that each neutron simulated corresponds to 4.6×10^4 EOT.

Stage II - Inside of our GEANT simulation, neutrons were emitted from 1 MeV to 1 GeV isotropically distributed outward 4 m into the concrete shield. In reality the maximum emission is 90 degrees from the beam direction[36] so these results, interpreted as isotropic in our simulation, will also be conservative. 5.1×10^7 such neutrons were emitted and tracked by our GEANT simulation. 1,072 neutrons crossed a vertical plane in the dirt 235 cm from the concrete shield. The location of these neutrons is shown in Figure XXX along with their energy spectrum.

a) b)

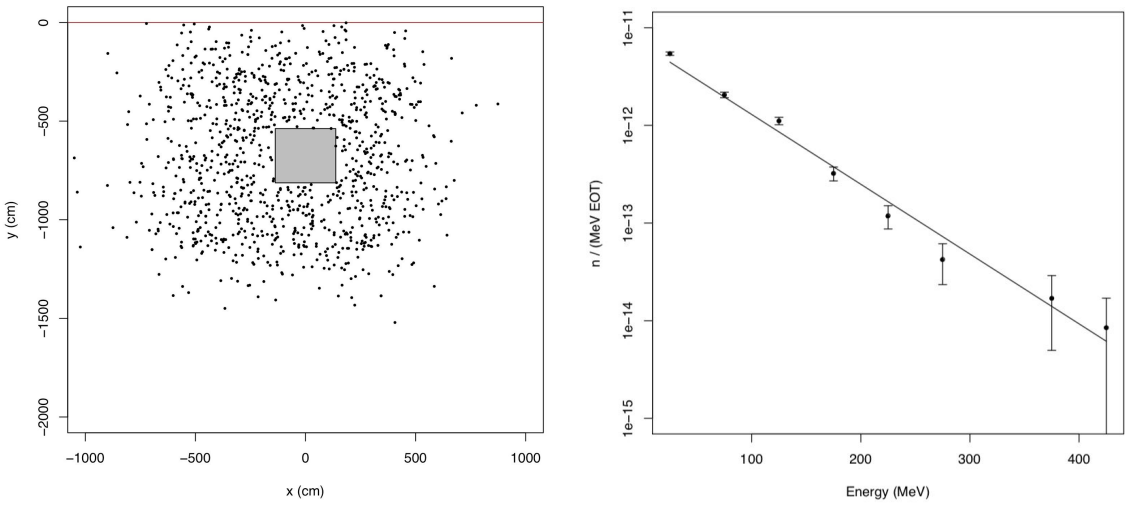

Figure XXX - a) Plot of xz coordinates of 1,072 neutrons passing a dirt plane 235 cm from the beam dump. The square in the middle is the iron shielding. The brown horizontal line shows ground level. b) Spectrum of neutron energies at the dirt plane.

For the next stage we simulate these neutrons. Each neutron simulated in Stage III represents at least 2.2×10^9 EOT.

Stage III - For this stage 6.0×10^7 neutrons were emitted from a dirt slab shown in Figure XXX a) with an energy distribution shown with the fit in Figure XXX b) out to 12 GeV and a forward-peaked angular distribution derived from the 1,702 recorded neutrons. 221 neutrons

crossed the walls into the experimental area surrounding BDX and BDX-DRIFT. The energies of these neutrons ranged up to 300 MeV. The appearance of neutrons in this energy range is consistent with a highly suppressed neutron interaction cross section at ~200 to ~300 MeV [38] with most elements. For the next stage we simulate these neutrons. Each neutron simulated in Stage IV represents at least 6.0×10^{14} EOT.

Stage IV - For this stage 2.5×10^{6} neutrons were emitted from the walls of the area surrounding the experimental area. 118 recoils were recording in the fiducial volume of a BDX-DRIFT-1m detector at 25× nominal pressure. Extrapolating we expect 315 recoils in BDX-DRIFT-10m detector during an exposure of 10^{22} EOT. Applying a 99% veto efficiency we find 0.1 events within 10 cm of the beam line for the entire exposure.

Summary of Background Estimates

Table 2 summarizes the conservative background estimates discussed in detail above. The first column indicates the source of the background, cosmic rays or beam. The second column shows the intermediate particle considered to produce the background recoils. The third column shows the number of events above threshold for a run of 10^{22} EOT within 10 cm of the beamline and assuming the veto efficiency shown in the third column.

Table 2 - Summary of Background Estimates

Source	Particle	Veto Efficiency	N per 10^{22} EOT
Cosmic Rays	μ	99.9%	0.4
	n	99%	
	p	99%	
Beam	ν	0%	0.007
	μ	99.9%	0.01
	n	99%	0.1

Signatures

Position

$\chi\bar{\chi}$ pairs are produced by decay of the *A'* particle as shown in Fig. XXX. Assuming the mass of the *A'* particle is much less than the beam energy, the decay will occur in a center of mass

(CM) at high velocity with respect to the lab frame. Thus $\chi\bar{\chi}$ pairs will be forward-peaked and because of the proximity of the detector to the beam-dump, the recoil event profile is expected to fall off rapidly from the beam line. For fixed beam energy, the higher the mass of the *A'* particle the lower the velocity of the CM where the decay into dark matter particles occurs and therefore the less forward peaked they will be. Figure XXX shows simulations of $\chi\bar{\chi}$ production, including beam scattering in the beam dump [28], for various dark matter masses assuming $m_{A'} = 3m_{\chi}$. The red boxes show the extent of the detector while the points represent the spread of the beam for various assumed m_{χ} masses. A simple measurement of recoil event position will yield a powerful signature of dark matter recoils, enable background suppression and provide information on dark matter mass.

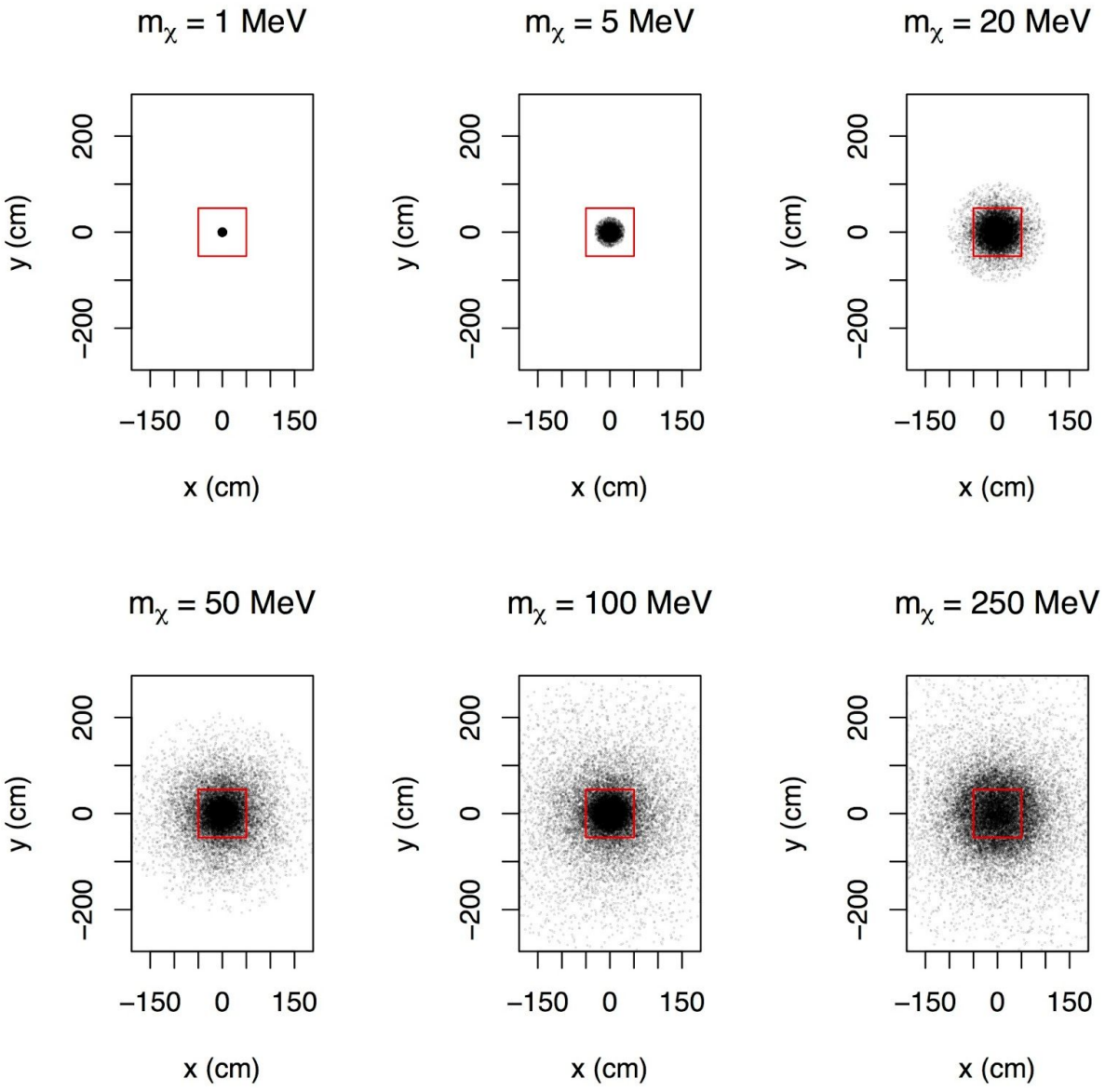

Figure XXX - These plots show the χ beam profile for various assumed dark matter masses at the detector location, shown in red.

Energy

The recoil energy spectrum of LDMA interactions is given by Equation (1). The response of the detector to neutron recoils generated by Cf-252 has been well modeled, see [24], including position and energy dependent efficiencies. Thus, the response of the detector to a LDMA signal can be accurately modeled and compared to the actual results providing another, energy, signature. Figure XXX shows a typical background NIPs spectrum. This one was generated for expected backgrounds for a BDX-DRIFT detector at JLab for the configuration shown in Figure XXX. The data are shown as black bars. In contrast, shown in varying colors, are the expected *NIPs* spectra for recoils from dark matter with various masses generated from Equation (1). All of the curves are roughly normalized to the same area as the background. As can be seen for low mass dark matter the spectra are significantly softer than the background while at high mass dark matter the spectra are significantly harder. For 0.02 GeV dark matter it would be hard to distinguish dark matter recoils from background recoils from just the ionization generated.

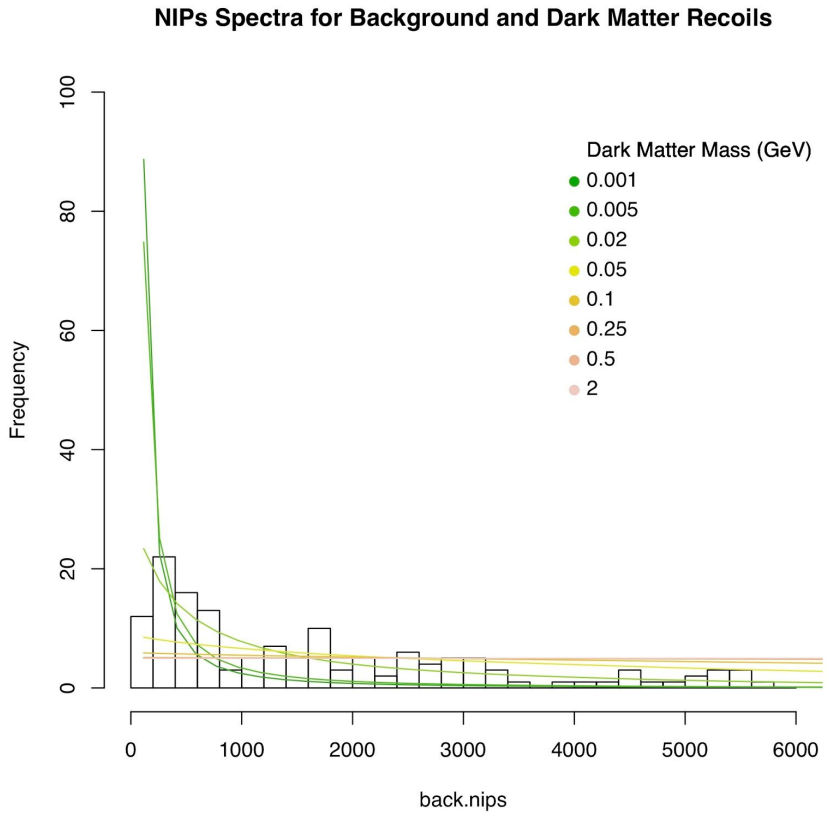

Figure XXX - This figure shows the recoil profile, NIPs, for a variety of light dark matter signatures and a background recoil profile associated with cosmic ray backgrounds.

Directional

The directional signature of LDMA recoils in a BDX-DRIFT detector arises from low energy S recoils which start out moving parallel to the readout planes as shown in Fig. XXX. Naively these events would have zero dispersion in *z* (drift direction) providing BDX-DRIFT with the strongest directional signature. Straggling of recoils at these low energies is, however, significant. Figure XXX(a) shows the result of a SRIM [22] simulation of 1,000 50 keV S recoils oriented, originally, perpendicular to the beam, or *z*, or horizontal direction. The signature, small dispersion in *z*, is degraded by straggling.

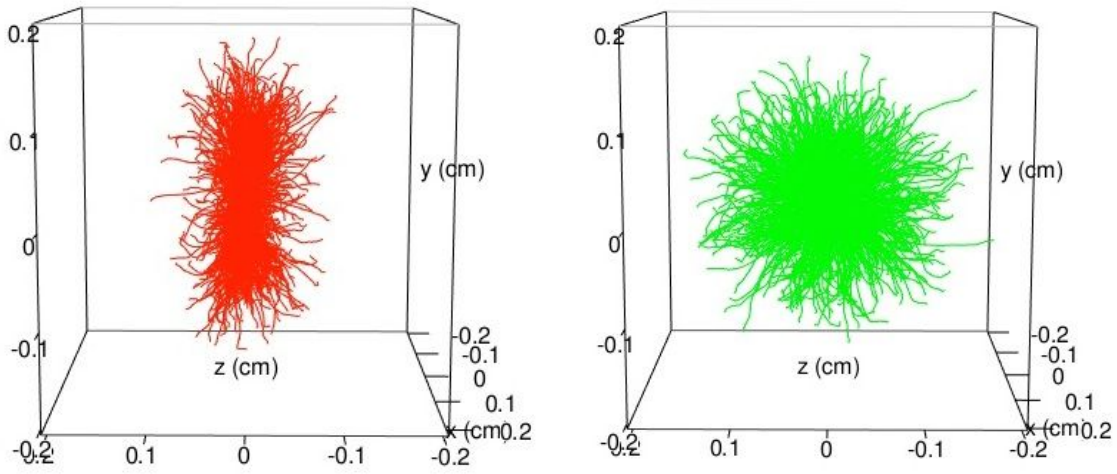

Figure XXX - (a) Tracks produced by 1,000 50 keV S recoils originally oriented perpendicular to the beam or z axis according to an SRIM [22] simulation. (b) Tracks produced by 1,000 50 keV S recoils oriented randomly as a comparison background. For scale the surrounding boxes are 4 mm in all dimensions.

For comparison Figure XXX(b) shows a SRIM simulation of 1,000 50 keV S recoils from cosmic ray or beam generated neutrons. These events are randomly oriented as expected from the physics of their generation and multiple bounces to enter the fiducial region and confirmed by GEANT simulations. For each event, signal or background, the dispersion of the ionization of the track in *z*, σ_z, was calculated including diffusion. The distributions are shown in Figure XXX. A Kolmogorov-Smirnov (KS) test then determined the probability that N_s signal events with N_b of background events was the same dispersion distribution as N_s + N_b background events. In order to produce a confidence limit (C.L.), this procedure was repeated multiple times with increasing N_s for fixed N_b. The number of signal events at

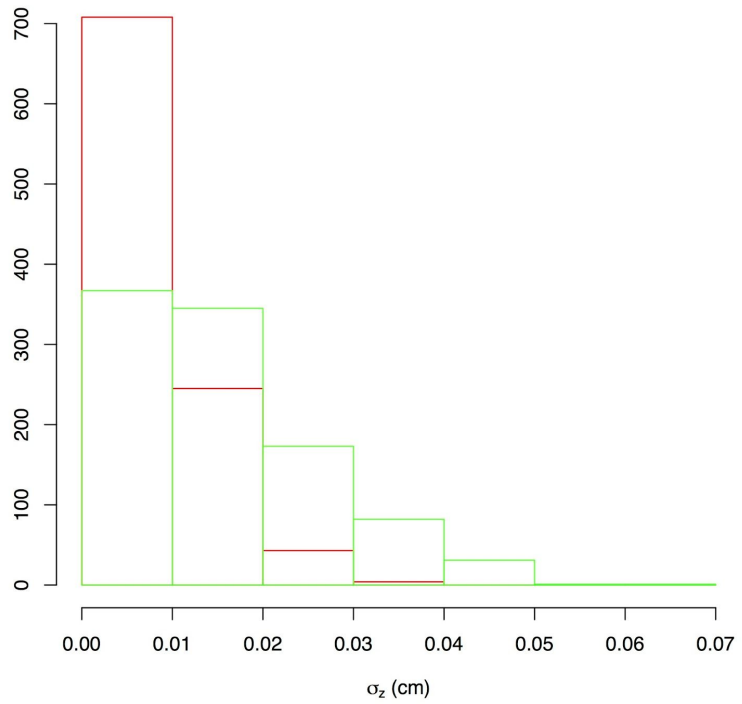

Figure XXX - Differences in the sigma z distributions for signal (red) and background (green) events.

which the KS test gave 10% or less probability of similarity 90% of the time was defined to be the 90% C.L. point. The black curves in Figure XXX show the number of signal events, N_s, required for a 90% C.L. detection in the presence of N_b background events for three S recoils threshold energies. For zero-background, 16 events would be required at 50 keV recoil energy. But even in the presence of 100 background events, in the area of the detector where signal events are expected, see Figure XXX, a significant detection can be found by running the detector only a few times longer than is required for zero background. This is due to the strong directional signature.

Thermal diffusion and various detector effects will contribute to the measured dispersion in z as well [15]. The largest of these is thermal diffusion from a track 50 cm from the detector plane. Fortunately, because the absolute position of the event, *z* can be measured and this contribution to the measured dispersion can be subtracted in quadrature [15]. Various detector contributions can also be removed based on [15], though the residual resolution, after subtraction, has yet to be fully characterized. The green (0.02 cm) and red (0.05 cm) curves in Figure XXXX show the effect of adding unaccounted, residual dispersion to the theoretical data.

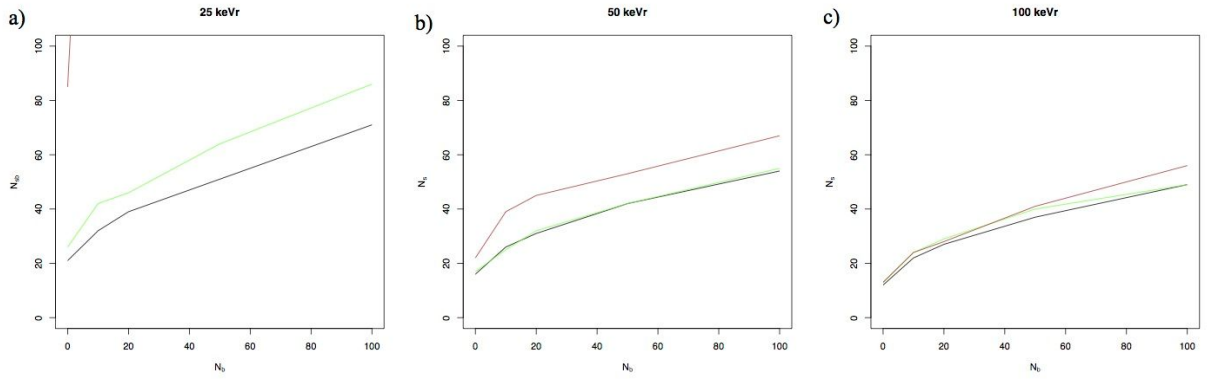

Figure XXX - The figures above show the number of signal events, N_s, on the vertical axis required for a 90% C.L. detection in the presence of, N_b, background events for three different recoil energies. The black curves are for perfect detector residual resolution, see text. The green curves are for a residual resolution of 0.02 cm. And the red curves are for a residual resolution of 0.05 cm.

R&D Needed

Some R&D will be needed before BDX-DRIFT can be deployed at JLab.

NITPC Readout Development

The development envisioned to run a BDX-DRIFT-10m detector is a continuation of development that has been ongoing for many years. A brief review is provided below.

DAQ v1 - The DRIFT collaboration employs a grouped-wire DAQ to lower costs at the expense of noise and information. The anode wires are divided into 8 groups, where group 1 includes wire 1, 9, 17, …; group 2 includes wire 2, 10, 18, … and so on. Each group of 56 wires is connected to a charge preamplifier, followed by a shaper, see Figure XXX. When the signal exceeds a preset threshold, the digitized signal is sent to a database for subsequent analysis. In addition, there is a 9^{th} channel to veto events taking place on the outer boundaries of the anode plane. Similarly, the grid wires consist of a 9-channel grouped acquisition. The entire detector requires 36 channels. In addition, the grid circuitry includes decoupling capacitors to remove the high voltage component from the signal. The digitizer runs at 1 MS/s. More details about this DAQ are detailed in [39].

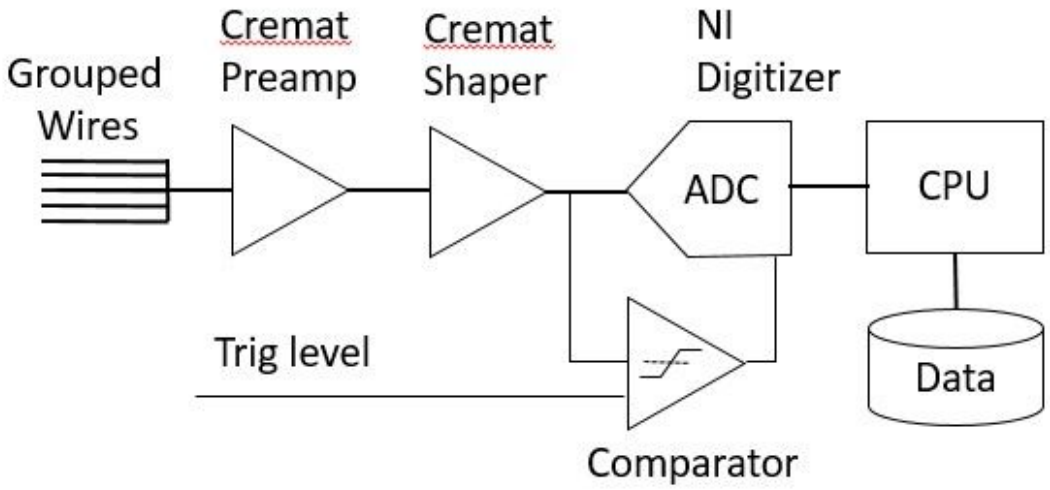

Figure XXX - Block diagram of DAQ v1.

This DAQ costs approximately $700 per channel and because of the grouping, has approximately 6,000 electrons equivalent noise charge (ENC). The grouping inherent in this system would not allow us to see the powerful position signature in a BDX-DRIFT experiment. Also the large noise prevents us from lowering our threshold down to the 20 keV utilized in our sensitivity plot. For all of these reasons (money, noise and grouping) development of the readout would be required to carry out the BDX-DRIFT experiment as planned.

DAQ v2 - The Occidental group has designed and built a new NITPC DAQ to address these concerns. The goal was to instrument all 2,048 wires of the DRIFT detector in order to reduce noise and gain information on the location of the events. They used an ASIC developed at Brookhaven National Laboratory (BNL) as charge preamplifiers [40][41]. Each chip handled 16 channels and included a shaper. The gain and peaking time were programmable. Each signal was fed to an ADC and the resulting digital signal was sent to a circular buffer until an event above threshold is detected. At that point, the trace and its time-stamp were transferred, via USB, to a host computer and stored in a database as shown in Figure XXX. All electronics were located in the vessel, using a single USB line and a few power lines to the outside. This system used an Arduino Due as CPU. The system was quite bulky, was limited in event rate, lacks flexibility, and had higher noise than expected due to cross-talk between channels. It was not designed to trigger on grid wires and yet this capability would be highly desirable.

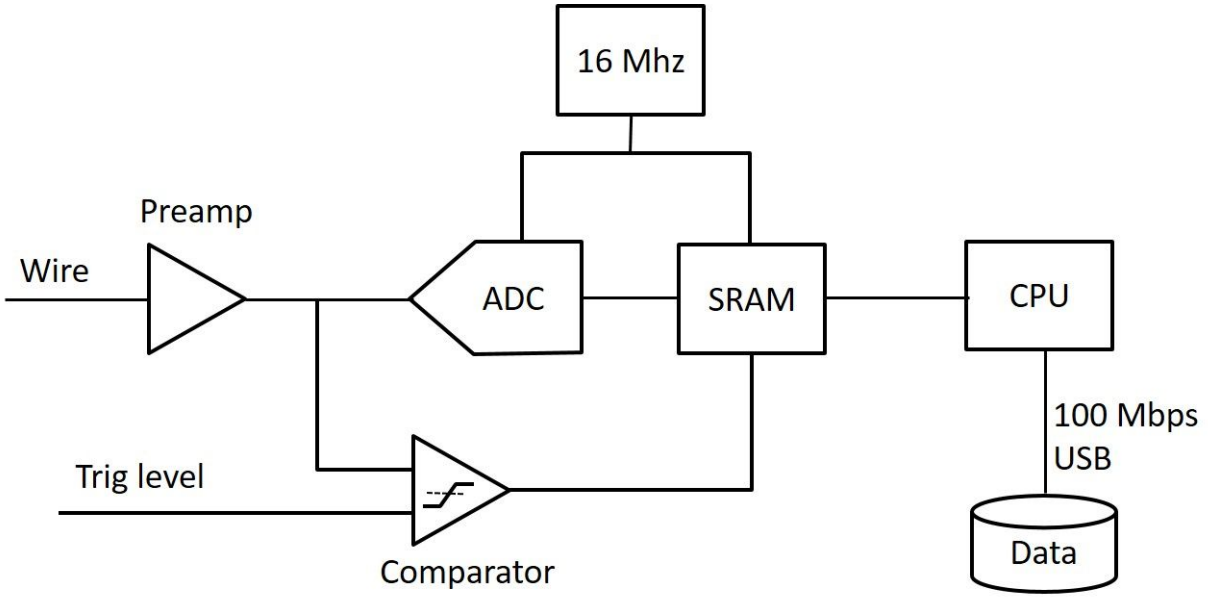

Figure XXX - Block diagram for DAQ v2.

The system ran at 1 MS/s, using 12 bit ADCs. The ADC could, in principle, resolve a charge as low as 110 electrons but we were limited by the capacitive noise of the circuit board and detector to about 750 e^- ENC. Cross talk between the lines increased the noise by another factor 3 (2,250 e^- ENC). It could collect up to 16 ms of data per channel, although only a few ms are necessary in practice. The detection was asynchronous, which means that the system scanned all wires independently for triggered lines and then handled them independently. Each triggered wire, automatically also triggered its immediate neighbor. For example, if wire 2,3,4 had a signal above threshold, the signals from wires 1,2,3,4,5 would be collected as extra wires have proven useful for analysis[15]. This system was limited to the 2 immediate neighbors being triggered. Occidental recently used this system to instrument 480 wires at a cost of ~$30 per channel.

Figure XXX show the DAQ v2 acquisition and preamplifier boards respectively.

a) b)

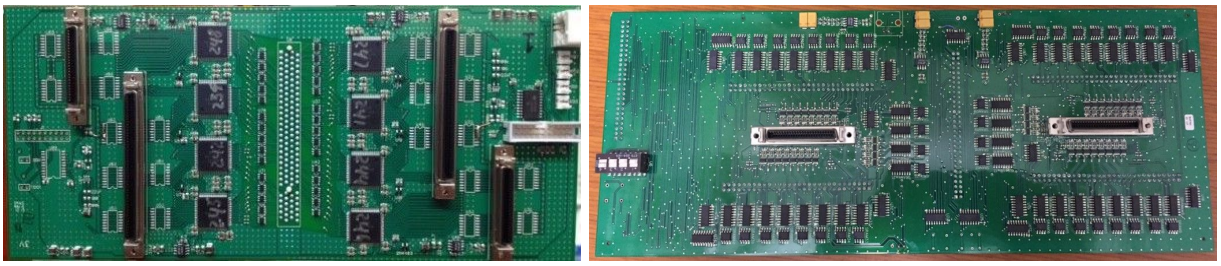

Figure XXX - a) Oxy/BNL 120 channel front-end board. b) Oxy 40 channel digital acquisition board.

Figure XXXa shows a neutron event on DRIFT-IIe. This detector had interspersed anode and grid, or field wires, spaced at 1 mm. Figure XXXb shows an alpha event on DRIFT-IIe. Both events illustrate typical data taken with the DAQ v2.

a) b)

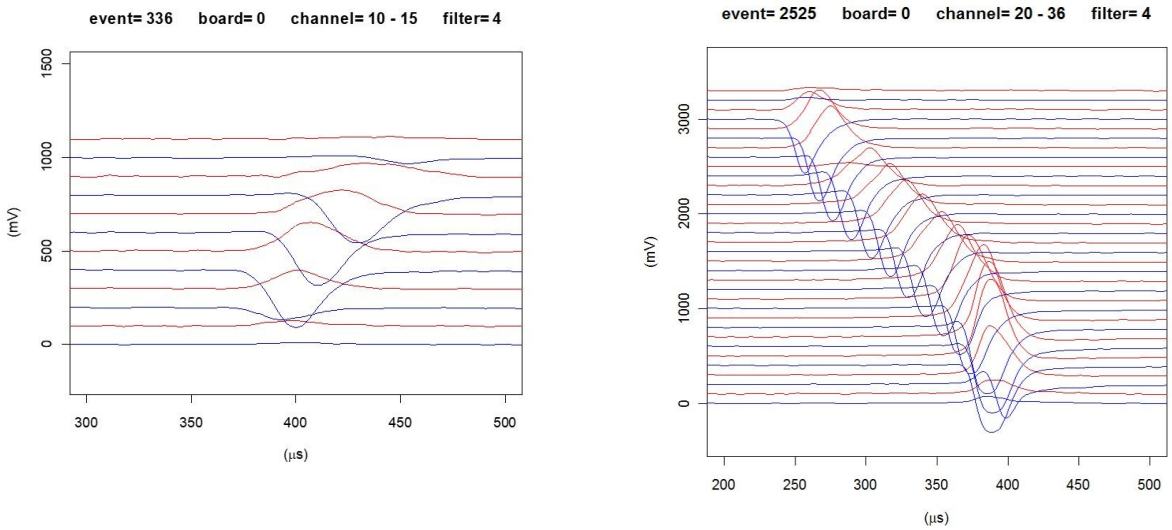

Figure XXX – a) A neutron event on DRIFT-IIe with interspersed anode and field wires. Blue is anode, red is field wire. Some digital filtering was used to remove noise. b) An alpha event in DRIFT-IIe. All events taken with a non-minority carrier gas.

DAQ v3 - The development work would include the fabrication of new preamplifier boards with differential signals, developing decoupler boards for the grid wires, and with the ability to withstand 3 kV, the fabrication of cards with 128 channels of simultaneous ADC, the configuration of a commercial FPGA board that would receive 128 channels of data and selectively transfer data that exceed the chosen threshold to a database. Many FPGAs are available on the market. The most popular chips exist on development boards. Such a board would save us time for design and fabrication if one is found that fit our needs. Figure XXX shows a block diagram of such a system. Again, all electronics would be inside the vessel, with only an Ethernet line and a few power lines connected to the outside, keeping penetrations to a minimum.

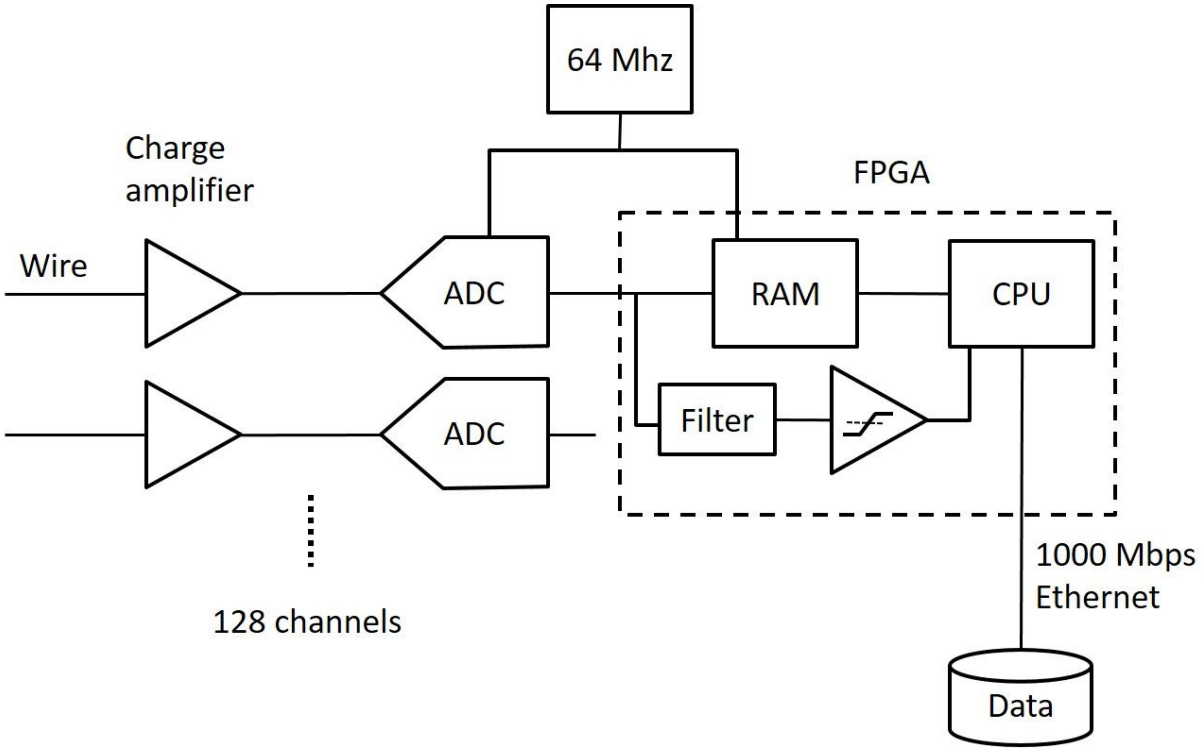

Figure XXX - Block diagram for DAQ v3

We have built a first version of preamplifiers in a collaboration of BNL. Here, DAQ v3 would simply upgrade the boards with the latest generation of preamplifiers available from BNL and would make use of differential signals to better control the noise. We also have experience building decoupler boards that can withstand 1 kV on each channel. This version would upgrade the capacitors to at least 3 kV.

DAQ v2 used 1 MS/s ADCs fabricated by Linear Technology (now Analog Devices). This version will use ADCs made by the same company, but able to digitize at up to 1.5 MHz a total of 8 channels simultaneously of analog signals. It will have a smaller footprint than DAQ v2, and it would accept the differential signals from the preamplifiers.

In DAQ v2 discrete components were used to trigger the system and store the data. DAQ v3 seeks to replace all of that with an FPGA. As shown in Figure XXX, the FPGA would store the signals in internal SRAMs and would create an event when a signal exceeds the chosen threshold. Because the FPGA is a programmable device, it would be straightforward to have a version that triggers on the inverted signals produced by the grid wires, instantly solving that problem. Typically, 1,000 samples pre-trigger and 1,000 samples post-trigger would be collected, for a total of 2 ms. This data and the time stamp would be transferred to a database via Ethernet communication. It would be possible to increase the number of samples per channel by decreasing the number of channels or by adding external dedicated SRAM for each channel. As an example, the Altera Cyclone V SE System-on-Chip combines an FPGA and a hard processor and can be found on development boards. A custom ADC board would be connected to such a development board to have a compact DAQ. With 16 such compact

DAQs we would be able to read 2,048 wires. An external clock would be required to keep each FPGA in sync.

Our goal with DAQ v3 is to demonstrate a price as low as $12 per channel, down from $30 per channel with our v2 DAQ, and noise down to 750 e^- ENC, down from 2,250 e^- ENC with our v2 DAQ and every wire read out to achieve access to lower thresholds and the ability to utilize the position signature in a search for LDM at JLab.

Scintillator veto

We calculate only 5% deadtime due to cosmic ray muons. Efficiency of the veto will depend on photocathode efficiency and coverage on the veto walls, and 10% coverage or better with highly reflective walls has been shown to be effective [29][32]. Detailed simulation work backed by measurements in conjunction with cost and safety considerations will be required to pin down an exact number but we expect >99.9% veto efficiency based on these initial estimates, reducing beam-unrelated backgrounds to less than 0.3 events within 10 cm of the beam line for the entire 10^{22} EOT exposure.

Proposals for both of these R&D efforts have been submitted to the DOE and ...

Conclusion

References

[1] P. Cushman *et al.*, “Snowmass CF1 Summary: WIMP Dark Matter Direct Detection,” *arXiv*, vol. 1310.8327, Oct. 2013.

[2] D. Bauer *et al.*, “Dark matter in the coming decade: Complementary paths to discovery and beyond,” *Phys. Dark Universe*, vol. 7–8, pp. 16–23, Mar. 2015.

[3] M. Battaglieri *et al.*, “US Cosmic Visions: New Ideas in Dark Matter 2017: Community Report,” *arXiv*, vol. 1707.04591, Jul. 2017.

[4] J. Alexander *et al.*, “Dark Sectors 2016 Workshop: Community Report,” *arXiv*, vol. 1608.08632, Aug. 2016.

[5] R. Essig *et al.*, “Dark Sectors and New, Light, Weakly-Coupled Particles,” *arXiv*, vol. 1311.0029, Oct. 2013.

[6] J. D. Bjorken *et al.*, “Search for neutral metastable penetrating particles produced in the SLAC beam dump,” *Phys. Rev. D*, vol. 38, no. 11, pp. 3375–3386, Dec. 1988.

[7] M. Diamond and P. Schuster, “Searching for Light Dark Matter with the SLAC Millicharge Experiment,” *Phys. Rev. Lett.*, vol. 111, no. 22, p. 221803, Nov. 2013.

[8] S. S. Chakrabarty and I. Jaeglé, “Search for dark photon, axion-like particles, dark scalar, or light dark matter in Compton-like processes,” *arXiv*, vol. 1903.06225, Mar.

2019.
[9] E. Izaguirre, G. Krnjaic, P. Schuster, and N. Toro, “Physics motivation for a pilot dark matter search at Jefferson Laboratory,” *Phys. Rev. D*, vol. 90, no. 1, p. 014052, Jul. 2014.
[10] M. Battaglieri *et al.*, “Measurements of the muon flux produced by 10.6 GeV electrons in a beam dump,” *Nucl. Instrum. Methods Phys. Res. Sect. Accel. Spectrometers Detect. Assoc. Equip.*, vol. 925, pp. 116–122, May 2019.
[11] G. Arcadi *et al.*, “The waning of the WIMP? A review of models, searches, and constraints,” *Eur. Phys. J. C*, vol. 78, no. 3, p. 203, Mar. 2018.
[12] S. Ahlen *et al.*, “The case for a directional dark matter detector and the status of current experimental efforts,” *Int. J. Mod. Phys. A*, vol. 25, no. 01, pp. 1–51, Jan. 2010.
[13] J. B. R. Battat *et al.*, “Readout technologies for directional WIMP Dark Matter detection,” *Phys. Rep.*, vol. 662, pp. 1–46, Nov. 2016.
[14] D. P. Snowden-Ifft, C. J. Martoff, and J. M. Burwell, “Low pressure negative ion time projection chamber for dark matter search,” *Phys. Rev. D*, vol. 61, no. 10, p. 101301, Apr. 2000.
[15] D. P. Snowden-Ifft and J.-L. Gauvreau, “High precision measurements of carbon disulfide negative ion mobility and diffusion,” *Rev. Sci. Instrum.*, vol. 84, no. 5, p. 053304, May 2013.
[16] C. J. Martoff, D. P. Snowden-Ifft, T. Ohnuki, N. Spooner, and M. Lehner, “Suppressing drift chamber diffusion without magnetic field,” *Nucl. Instrum. Methods Phys. Res. Sect. -Accel. Spectrometers Detect. Assoc. Equip.*, vol. 440, no. 2, pp. 355–359, Feb. 2000.
[17] T. Ohnuki, D. P. Snowden-Ifft, and C. J. Martoff, “Measurement of carbon disulfide anion diffusion in a TPC,” *Nucl. Instrum. Methods Phys. Res. Sect. -Accel. Spectrometers Detect. Assoc. Equip.*, vol. 463, no. 1–2, pp. 142–148, May 2001.
[18] W. Blum and L. Rolandi, *Particle detection with drift chambers*, Springer study ed. Berlin ; New York: Springer-Verlag, 1994.
[19] S. Burgos *et al.*, “Measurement of the range component directional signature in a DRIFT-II detector using 252Cf neutrons,” *Nucl. Instrum. Methods Phys. Res. Sect. Accel. Spectrometers Detect. Assoc. Equip.*, vol. 600, no. 2, pp. 417–423, Mar. 2009.
[20] J. B. R. Battat *et al.*, “First measurement of nuclear recoil head-tail sense in a fiducialised WIMP dark matter detector,” *J. Instrum.*, vol. 11, no. 10, pp. P10019–P10019, Oct. 2016.
[21] D. Spergel, “Motion of the Earth and the Detection of Weakly Interacting Massive Particles,” *Phys. Rev. D*, vol. 37, no. 6, pp. 1353–1355, Mar. 1988.
[22] J. F. Ziegler, M. D. Ziegler, and J. P. Biersack, “SRIM – The stopping and range of ions in matter (2010),” *Nucl. Instrum. Methods Phys. Res. Sect. B Beam Interact. Mater. At.*, vol. 268, no. 11, pp. 1818–1823, Jun. 2010.
[23] J. B. R. Battat *et al.*, “Measurement of directional range components of nuclear recoil tracks in a fiducialised dark matter detector,” *J. Instrum.*, vol. 12, p. P10009, Oct. 2017.
[24] J. B. R. Battat *et al.*, “Low threshold results and limits from the DRIFT directional dark matter detector,” *Astropart. Phys.*, vol. 91, pp. 65–74, May 2017.
[25] S. Burgos *et al.*, “Studies of neutron detection and backgrounds with the DRIFT-IIa dark matter detector,” *Astropart. Phys.*, vol. 28, no. 4–5, pp. 409–421, Dec. 2007.
[26] D. P. Snowden-Ifft, T. Lawson, N. J. C. Spooner, and N. Villaume, “Low energy alphas in the drift detector,” *Nucl. Instrum. Methods Phys. Res. Sect. -Accel. Spectrometers Detect. Assoc. Equip.*, vol. 516, no. 2–3, pp. 406–413, Jan. 2004.
[27] D. P. Snowden-Ifft, “Discovery of multiple, ionization-created CS2 anions and a new mode of operation for drift chambers,” *Rev. Sci. Instrum.*, vol. 85, no. 1, p. 013303, Jan.

2014.
[28] A. Celentano (Private Communication), “Re: Files,” 08-Oct-2018.
[29] E. Aguayo Navarrete, R. T. Kouzes, A. S. Ankney, J. L. Orrell, T. J. Berguson, and M. D. Troy, “Cosmic Ray Interactions in Shielding Materials,” Pacific Northwest National Lab. (PNNL), Richland, WA (United States), PNNL-20693, Sep. 2011.
[30] S. Agostinelli *et al.*, “Geant4—a simulation toolkit,” *Nucl. Instrum. Methods Phys. Res. Sect. Accel. Spectrometers Detect. Assoc. Equip.*, vol. 506, no. 3, pp. 250–303, Jul. 2003.
[31] S. Dazeley, A. Bernstein, N. S. Bowden, and R. Svoboda, “Observation of neutrons with a Gadolinium doped water Cherenkov detector,” *Nucl. Instrum. Methods Phys. Res. Sect. Accel. Spectrometers Detect. Assoc. Equip.*, vol. 607, no. 3, pp. 616–619, Aug. 2009.
[32] M. Sweany *et al.*, “Large-scale gadolinium-doped water Cherenkov detector for nonproliferation,” *Nucl. Instrum. Methods Phys. Res. Sect. Accel. Spectrometers Detect. Assoc. Equip.*, vol. 654, no. 1, pp. 377–382, Oct. 2011.
[33] S. Westerdale, E. Shields, and F. Calaprice, “A prototype neutron veto for dark matter detectors,” *Astropart. Phys.*, vol. 79, pp. 10–22, Jun. 2016.
[34] K. Scholberg, “Prospects for measuring coherent neutrino-nucleus elastic scattering at a stopped-pion neutrino source,” *Phys. Rev. D*, vol. 73, no. 3, p. 033005, Feb. 2006.
[35] L. Marsicano, M. Battaglieri, A. Celentano, R. De Vita, and Y.-M. Zhong, “Probing leptophilic dark sectors at electron beam-dump facilities,” *Phys. Rev. D*, vol. 98, no. 11, p. 115022, Dec. 2018.
[36] M. Tanabashi *et al.*, “REVIEW OF PARTICLE PHYSICS Particle Data Group,” *Phys. Rev. D*, vol. 98, no. 3, p. 030001, Aug. 2018.
[37] S. Taniguchi *et al.*, “Neutron energy and time-of-flight spectra behind the lateral shield of a high energy electron accelerator beam dump. Part I: measurements,” *Nucl. Instrum. Methods Phys. Res. Sect. -Accel. Spectrometers Detect. Assoc. Equip.*, vol. 503, no. 3, pp. 595–605, May 2003.
[38] W. P. Abfalterer, F. B. Bateman, F. S. Dietrich, R. W. Finlay, R. C. Haight, and G. L. Morgan, “Measurement of neutron total cross sections up to 560 MeV,” *Phys. Rev. C*, vol. 63, no. 4, p. 044608, Mar. 2001.
[39] G. J. Alner *et al.*, “The DRIFT-II dark matter detector: Design and commissioning,” *Nucl. Instrum. Methods Phys. Res. Sect. -Accel. Spectrometers Detect. Assoc. Equip.*, vol. 555, no. 1–2, pp. 173–183, Dec. 2005.
[40] G. De Geronimo *et al.*, “Front-End ASIC for a Liquid Argon TPC,” *Ieee Trans. Nucl. Sci.*, vol. 58, no. 3, pp. 1376–1385, Jun. 2011.
[41] H. Chen *et al.*, “Readout electronics for the MicroBooNE LAr TPC, with CMOS front end at 89K,” *J. Instrum.*, vol. 7, p. C12004, Dec. 2012.